YUNIBESITI YA BOKONE-BOPHIRIMA
NORTH-WEST UNIVERSITY
NOORDWES-UNIVERSITEIT

# THE FLUTTER ANALYSIS OF THE JS1 GLIDER

**PS Rossouw, B.Eng (Mech)**

Mini-dissertation submitted in fulfilment of the requirements for the degree Master of Engineering at the Potchefstroom campus of the North-West University

**Supervisor:** **Mr. AS Jonker**

**Potchefstroom**
**November 2007**

## *Abstract*

A flutter analysis of the new prototype 18-meter glass glider, the JS1 Revelation, was performed. The analysis was conducted in two main parts, a modal analysis done by a ground vibration test, followed by a flutter prediction.

A ground vibration test was performed on the glider in two configurations: with no water ballast and with water ballast in the wings. For each of these cases the $1^{st}$, $2^{nd}$ and $3^{rd}$ symmetric and anti-symmetric wing bending modes and wing torsion modes were extracted as well as fin, stabilizer and fuselage modes. All of these modes were extracted in the frequency range 1 Hz – 32 Hz. The natural frequency, modal damping and mode shape of each mode are among the modal results.

The flutter prediction was done with the software code SAF (Subsonic Aerodynamic Flutter). SAF makes use of a panel model of the glider and utilized the doublet lattice method and p-k flutter solution method. So far, results in the form of damping vs. velocity and frequency vs. velocity graphs indicated stability of main surface modes in the velocity range up to $1.2V_D$ up to an altitude of 8000 meters.

## *Uittreksel*

'n Fladder analise is gedoen op die nuwe 18 meter klas sweeftuig prototipe, die JS1 Revelation. Die analise is in twee hoof dele gedoen, nl. 'n modale analise uitgevoer deur 'n grond vibrasie toets, gevolg deur 'n fladder voorspelling.

`n Grond vibrasie toets is uitgevoer vir twee sweeftuig konfigurasies: sonder water en met water in die vlerk tenks. Vir elk van hierdie twee gevalle is die eerste, tweede en derde simmetriese en anti-simmetriese vlerk buig modes en vlerk torsie modes geïsoleer en die data daarvan onttrek sowel as die vin, stertvlerk en romp modes. Al hierdie modes is onttrek in die frekwensie reeks van 1 Hz tot 32 Hz. Die natuurlike frekwensie, modale demping en mode vorms van elke mode is onder die data wat onttrek is.

Die fladder voorspelling is uitgevoer met die sagteware kode SAF (Subsonic Aerodynamic Flutter). SAF maak gebruik van `n paneel model van die sweeftuig en gebruik die sogenaamde *doublet lattice* metode en die p-k oplossing metode. Resultate in die vorm van demping versus snelheid en frekwensie teen snelheid het sover stabiliteit getoon vir die hoof oppervlak modes in die snelheidsreeks tot by $1.2V_D$ en tot 'n hoogte van 8000 meter.

## *Acknowledgement*

I would like to thank my heavenly Father for the strength and insight during this study and He who is preparing me for His work. Thanks to my parents for their support and love. I would like to thank my supervisor, Attie Jonker, for the opportunity and guidance throughout this project. I would also like to thank the CSIR personnel for their help with the ground vibration test, in particular Louw van Zyl.

# Table of contents

## List of Figures

## *List of Tables*

# 1 INTRODUCTION

## 1.1 History

In the early days of flight there was a great spirit of adventure that prevailed and this encouraged aviators to take great risks. As airspeeds started to increase, a new problem developed. Aircraft encountered a phenomenon by which they would start to vibrate violently. This phenomenon was little understood before the 1930's. For an aircraft to fly, it has to have a lightweight structure. This weight restriction reduces the stiffness of the structure. Static air loads on a wing are always less than the structural strength. When the wings start to twist and bend in a periodic manner, under certain conditions, dynamic air loads can cause the elastic motion to grow in amplitude. In turn, this causes increased air loads and eventually the structural strength is exceeded. This coupling between the elastic motion and unsteady aerodynamic loading is called flutter (Tewari, 1999).

The first recorded flutter incident was on a Handley Page O/400 twin-engine biplane bomber in 1916 (Kehoe, 1995:1). To avoid flutter problems, early aircraft used extensive wire bracing to support and stiffen the structure (Hollmann, 1997:3). As better engines became available, airplanes flew faster, trying to set new flying records. In addition, after World War I, there was a shift from external wire-braced biplanes to cantilevered wings, which resulted in more wing flutter incidents. There were no formal flutter testing of full-scale aircraft and aircraft simply flew to its maximum speed to demonstrate it to be free of flutter. The first papers on flutter appeared in 1924. The first formal flutter test was carried out by Von Schlippe in 1935. The test was to vibrate the aircraft at resonant frequencies at progressively higher speeds and plot amplitude as a function of airspeed. If there were a rise in amplitude, it would suggest reduced damping with flutter occurring at the asymptote of theoretically infinite amplitude. The idea was successfully applied to several German aircraft until, a Junkers JU90 fluttered and crashed during flight tests in 1938 (Kehoe, 1995:1).

At that time, engineers had inadequate instrumentation, excitation methods, and stability determination techniques. However, as the World Wars demanded faster aircraft and flutter became more of a problem, serious efforts in analysing and preventing flutter began in earnest. Over the years, flight flutter testing techniques, instrumentation, and response data analysis saw considerable improvements (Kehoe, 1995:1). Analytical methods for predicting flutter were also developed and with the development of mainframe computers in the early 1970's, aerospace companies within the United States began developing computer programs

capable of more accurately predicting flutter. A program, titled FASTOP, for Flutter And STrength Optimization Program, developed in 1973, is one such a program. In 1980 and 1981, the updated and reorganized program resulted as the code FASTEX. Both government and industry has used FASTEX extensively. In 1991, FASTEX was modified to run on a personal computer and SAF, Subsonic Aerodynamic Flutter, was born (Hollmann, 1997:4).

Aircraft Designs, Inc., for which FASTEX was modified, used SAF ever since to predict the critical flutter speed of aircraft. This study also utilised SAF to predict the critical flutter speed of the JS1 glider.

## *1.2 Problem definition*

For the past 10 years or so, a design team at Jonker Sailplanes with the North-West University in South Africa developed a new composite 18m class glider called the JS1. Part of the certification for the glider is to show that it is free from flutter within its design envelope.

To proof this, an analytical flutter analysis and flutter tests must be performed. A preliminary theoretical flutter analysis (De Bruyn, 2004) was already done on the JS1. At the time of that study, the glider was still in the design stage. By the time of this study, the manufacturing of the glider had already started. The next step in the analysis is then to do an experimental investigation. With the glider built, data can now be retrieved from tests using the actual glider. The problem is therefore to investigate the structural response of the JS1 glider experimentally and define the critical flutter speed.

## *1.3 Objectives of study*

The main objective of this study is to determine the critical flutter speed of the JS1 glider. The analysis would include the main lifting surfaces and control surfaces. The whole flutter analysis consists of two main procedures, the modal analysis, and the flutter prediction.

Modal analysis is the process of determining the dynamic characteristics of a vibrating system. The dynamic characteristics needed in the flutter analysis are the mode shapes and modal parameters. The modal parameters consist of the natural frequencies and damping ratios associated with each of the mode shapes. A modal analysis is performed by use of an analytical method or ground vibration test (GVT). Since an analytical method was used in the preliminary study using a finite element analysis to determine the dynamic characteristics, a

GVT will be performed for a more accurate prediction of the dynamic characteristics. Results from the two approaches can then be compared.

With the dynamic characteristics of the glider determined and with the known geometric information of the glider, the flutter prediction code can be used to calculate the flutter speed. As mentioned in Section 1.1, the flutter prediction code that will be used in this study is SAF. The flutter prediction will be done for the main flying surfaces, which are the wings, fin, and tailplane of the glider.

## *1.4 Limitations*

The finite element model of the whole glider is not available since the software in which a model of the glider was created in the preliminary study is not available at the university any more. The only part of the glider, which was modelled in the new available finite element software, is the tailplane. Results for the other parts of the glider can still be compared to results from the preliminary study, but not to an updated finite element model.

## *1.5 Outline/Layout of study*

In the next chapter, regulations, and a literature overview of the methods used in a flutter analysis will be given. This includes the modal analysis and flutter prediction methods. Chapter 3 will discuss the experimental modal analysis done on the glider and results will be compared with the preliminary study results. In Chapter 4, the flutter prediction and the results found will be given and compared with that of the previous study. Chapter 5 will discuss the results and conclusion of the study.

# 2 LITERATURE STUDY

## 2.1 Introduction

Aeroelasticity is the field of study concerned with the mutual interaction among inertial (dynamics), elastic (solid mechanics), and aerodynamic (fluid mechanics) forces. Collar suggested that aeroelasticity could be visualized as forming a triangle of these disciplines (Dowell et al., 1995:1) illustrated by Figure 2.1. Other technical fields can be identified were these main fields pair.

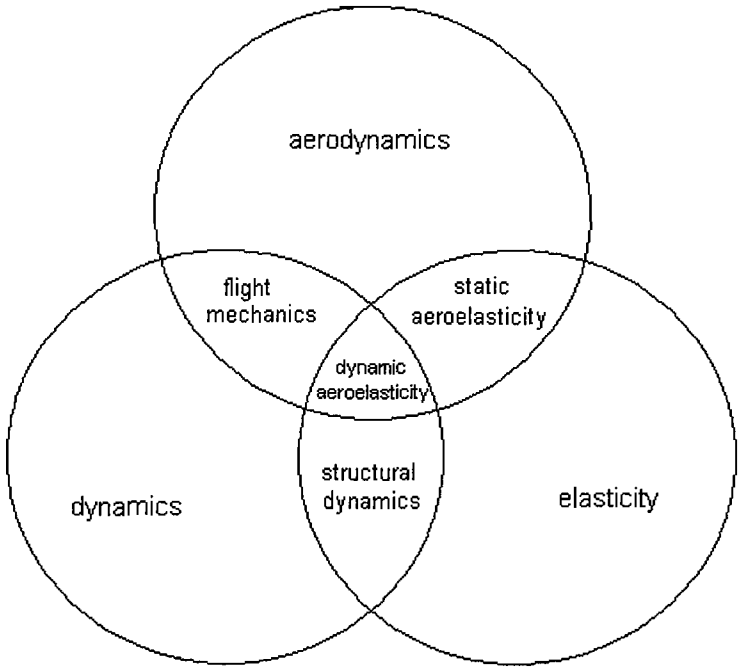


**Figure 2.1 Schematic illustration of the field of aerodynamics (Hodges&Pierce, 2002:2).**

The prediction of forces caused by fluids acting on a body of a given shape is provided by aerodynamic theories. Elasticity is the prediction of a shape of an elastic body under a given load. Dynamics studies the effects of inertial forces (Hodges & Pierce, 2002:1). Aerodynamic forces strongly depend on the elastic moduli of a given structural member. It can thus sometimes happen that the aerodynamic forces are greater than the elastic restoring forces. When this occurs and the inertial forces have little effect, it is refer to as static aeroelastic instability, or divergence. However, when the inertial forces are important, the resulting dynamic instability is called flutter (Hodges & Pierce, 2002:3). Both of these aeroelastic phenomena are of undesirable character leading to loss of effectiveness or even sometimes spectacular structural failure as in the case of aircraft flutter. It is thus clear why so much

research had been done and so many reports was written and is still written to try to explain, understand and prevent flutter. Although flutter test techniques have advanced, today's techniques are still based upon the three components of Von Schlippe's method: structural excitation, response measurement, and data analysis for stability (Kehoe, 1995:4).

This chapter will look at the regulations applicable for the investigation of flutter and at the two main procedures in accomplishing the main objective of this study, namely the modal analysis and flutter prediction.

## 2.2 Regulations

As mentioned in the Problem identification, paragraph 1.2, the analysis for flutter, apart from assuring to build a safe aircraft, is for certification purposes. To certify an aircraft, there must be a compliance with certain regulations. The European Union's strategy for aviation safety is the European Aviation Safety Agency (EASA). The Agency is compiling the Certification Specifications (CS) with the co-operation of the Joint Aviation Authorities. The Airworthiness Authorities of certain European countries signed a document in March 1979 under which they agree to co-operate in agreeing common comprehensive airworthiness requirements, referred to as the Joint Aviation Requirements (JAR). CS under part 22 sets the requirements and specifications for sailplanes and powered sailplanes. The United States also have their own regulations namely the Federal Aviation Regulation (FAR). CS-22 would be used in this study.

CS-22 under section 22.629 describe the specifications to which a sailplane or glider has to comply with. It states in sub-paragraph (a):

*"The sailplane must be free from flutter, aerofoil divergence, and control reversal in each configuration and at each appropriate speed up to at least $V_D$. Sufficient damping must be available at any appropriate speed so that aeroelastic vibration dies away rapidly."* (CS, 2003:1-D-2).

Compliance is shown by a ground vibration test and includes an analysis and evaluation of the modes and frequencies found in the GVT. The purpose of the evaluation is to determine possible combinations of modes, which could be critical for flutter. An analytical method must determine any critical speed in the range up to 1.2 times the design diving speed, $V_D$. In addition, to comply with sub-paragraph (a), flight tests to induce flutter at speeds up to the demonstrated flight diving speed, $V_{DF}$, to show that a suitable margin of damping is available

with no rapid reduction in damping as $V_{DF}$ is approached. The flight test must also show that control effectiveness around all three axes is not decreasing in an unusually rapid manner as $V_{DF}$ is approached. There must be no signs of approaching aerofoil divergence of wings, tailplane, and fuselage, which can result from the trend of the static stabilities and trim conditions (CS, 2003:1-D-2).

The design diving speed of the JS1 glider is 324 km/h. The analysis must thus show the requirements mentioned in the previous paragraph to speeds up to 388.8 km/h. The focus of this study is only on the GVT and not on the flight-testing.

## *2.3 Modal analysis*

Modal analysis is about the determination of the natural frequencies, damping ratios and mode shapes of a vibrating structure. The natural frequency of a structure is where a structure starts to resonate, i.e. when the structure oscillates with large displacements. The forcing frequency is here the same as the natural frequency and the damping is not large. When a structure vibrates, the vibration energy gradually converts into heat and sound and this is known as damping. Damping thus limits the amplitude of vibration (Rao, 2004:685). Mode shapes are the way in which a structure vibrates (displacements of a structure) and is different for every natural frequency.

Modal analysis, also known as experimental modal analysis, is done by physically measuring the dynamic characteristics with certain hardware. This hardware is used when a GVT is performed. However, the natural frequencies and mode shapes could also be determined by a finite element analysis (FEA). The finite element method (FEM) has been incorporated in several computer software and is a powerful tool for static and dynamic structural analysis.

A FEA of the aircraft is thus the first step in determining natural frequencies and mode shapes of a structure. This is done before an aircraft is built. A flutter prediction program then uses these dynamic characteristics to determine a critical flutter speed. After an aircraft is built, components are weighed and the FEM is updated. A GVT is performed on the completed aircraft and the dynamic characteristics of the aircraft are determined. These parameters are directly used in a flutter program. Results from the GVT and FEA can then be compared. Only the GVT can be performed as has been done in the past, but is not recommended (Hollmann, 1997:12).

The discussion of obtaining the modal parameters by analytical method, FEA, and by experimental method, GVT, follows next.

### 2.3.1 Analytical method

Natural frequencies and mode shapes can be determined by an analytical method. This method involves the use of a finite element analysis program. The FEM is first used to solve the structural problems of a structure. It is then used for the dynamic analysis i.e. to determine the eigenvalues (square of natural frequency) and eigenvectors (mode shapes). It can be shown (Rao, 2004:869), by using Lagrange's equations, that an equation of motion for a complete structure can be expressed as

$$[M]\ddot{\vec{x}} + [C]\dot{\vec{x}} + [K]\vec{x} = \vec{F} \tag{2.1}$$

[M] is the mass matrix, [C] the damping matrix and [K] the stiffness matrix. $\vec{F}$ is the load vector, $\vec{x}$ the displacement vector and $\dot{\vec{x}}$ and $\ddot{\vec{x}}$ the velocity and acceleration vectors. To solve this differential equation a general solution (Zienkiewicz & Taylor, 2000:485) can be written as

$$\vec{x} = \vec{X}\exp(\omega t) \tag{2.2}$$

Substituting equation (2.2) into equation (2.1) gives

$$\left(\omega^2[M] + \omega[C] + [K]\right)\vec{X} = \vec{F} \tag{2.3}$$

Solving equation (2.3) gives values for $\omega^2$ (eigenvalue) and vector $\vec{X}$ (mode shapes). $\omega$ is the natural frequency.

When the finite element model is created, it is important to set up the model accurately. Material stiffness and weights must be realistically modelled and control surface system stiffness accurately predicted. Accurate mass balancing of control surfaces about their hinge lines is also important. Hollmann (1997:9) describes that a weight difference of 142 gram on the aileron's mass balance weights reduced the flutter speed of new Lancair ES from 360 knots to 160 knots. When the building of the aircraft is complete, the mass and stiffness of the aircraft components can be weighed and determined and the FEM updated to reflect the true properties.

In a FEM, the modelled structure is divided into a finite number of elements. A structure is thus an assemblage of several finite elements. Different models with various numbers of elements are used to determine with what number of elements the results converge. With the FEM modelled as accurately as possible, it then gives a good prediction of the dynamic properties. Shokrieh (2001:6) obtained in their analysis "excellent agreement between the

analytical and experimental results". A FEA is thus a great asset during the design process of an aircraft.

## 2.3.2 Experimental method

When vibration is measured, one requires the following hardware (Rao, 2004:769):

- A source of excitation to apply a known input force to the structure.
- A transducer to convert physical motion into an electrical signal.
- A signal-conditioning amplifier to make the transducer characteristics compatible with the input electronics of the digital data acquisition system.
- And an analyzer to process signals and to do the modal analysis using suitable software.

These hardware components are discussed next.

### 2.3.2.1 Excitation

An electrodynamic shaker or an impact hammer may be used as an exciter. The impact hammer is a hammer with a built-in force transducer in its head. A wide range of frequencies can be excited when the structure is hit or impact by the impact hammer. It also rule out the problem of mass loading, which is the effect of influencing the measured response, such as the case with the electrodynamic shaker when it's attached to a structure. It is however difficult to control the direction of the applied force and not all surfaces can be impact tested. The reason may be that the structure has delicate surfaces or that the impacting force is not sufficient to adequately excite the modes of interest.

For large input forces, an electrodynamic shaker is used. It measures the response easily and the output of this shaker can be easily controlled. The vibration exciter or shaker is usually attached to the structure through a long slender rod to isolate the shaker from the structure, reduce the added mass and to apply the force along the axial direction of the rod. This rod is called a stinger. Between the structure and stinger, a transducer called a load cell is attached to measure the excitation force. Other types of shakers are of mechanical, electro dynamical and hydraulic type.

### 2.3.2.2 Transducers

Devices that transform values of physical variables into equivalent electrical signals are called transducers. Again, there are many types of transducers. The most popular are the

piezoelectric transducers. Quartz is an example of the material used in these transducers. It generates an electrical charge when subjected to a deformation of mechanical stress. It can be designed to produce signals proportional to either force or acceleration (Rao, 2004:770). Acceleration can also be measured by sensing the change in capacitance (MEMS accelerometers). The capacitance is converted to voltage so that a signal is produced. Force is measure by transducers called load cells. Force and acceleration can also be measured at the same time by using an impedance head. This is quite useful if the transfer function of a system must be calculated.

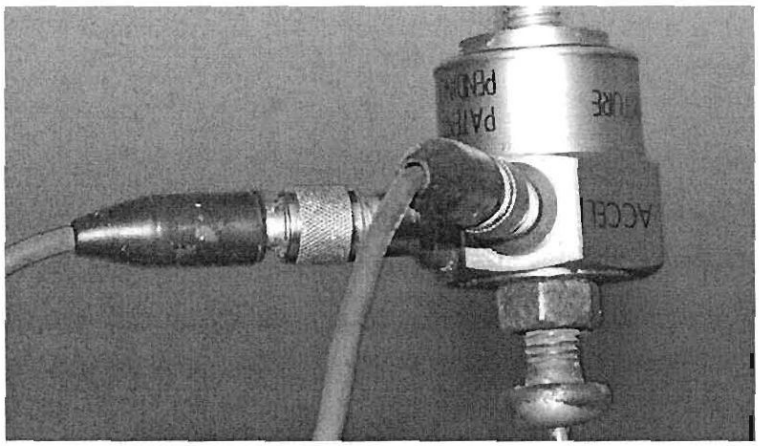

**Figure 2.2 An impedance head mounted to a structure with wires connected.**

### 2.3.2.3 Signal conditioner

Signal conditioners, in the form of charge or voltage amplifiers match and amplify the signals before signal analysis. This is because the output impedance of transducers is not suitable for direct input into the signal analysis equipment. In other words, the voltage signal from the transducer will be reduced by the capacitance of the cable connecting the transducer to the signal analysis equipment.

### 2.3.2.4 Data analysis

Digital frequency analyzers (also called spectrum analyzers) are used for signal processing. A commonly used analyzer is called the fast Fourier transform (FFT) analyzer. Voltage signals from a transducer (representing for example acceleration) go through a signal conditioning amplifier, filter, and digitizer. The FFT analyzer receives these signals for computations and transforms the digitally sampled time domain signals into a finite number of frequency components (discrete frequency spectra). These components are actually Fourier coefficients. Apart from this, the analyzer also computes cross-spectra between the input and the different

output signals. Natural frequencies, damping ratios and mode shapes can then be determined from the analyzed signals in numerical or graphical form.

The Fourier series expansion describes any periodic function as a sum of harmonic functions. The Fourier series can describe any periodic function using either a time domain or frequency domain representation. An example of harmonic function is $x(t) = A\sin\omega t$. Represented in the time domain is shown in Figure 2.3(a). Representing the function in the frequency domain by the amplitude and frequency $\omega$ is shown in Figure 2.3(b).

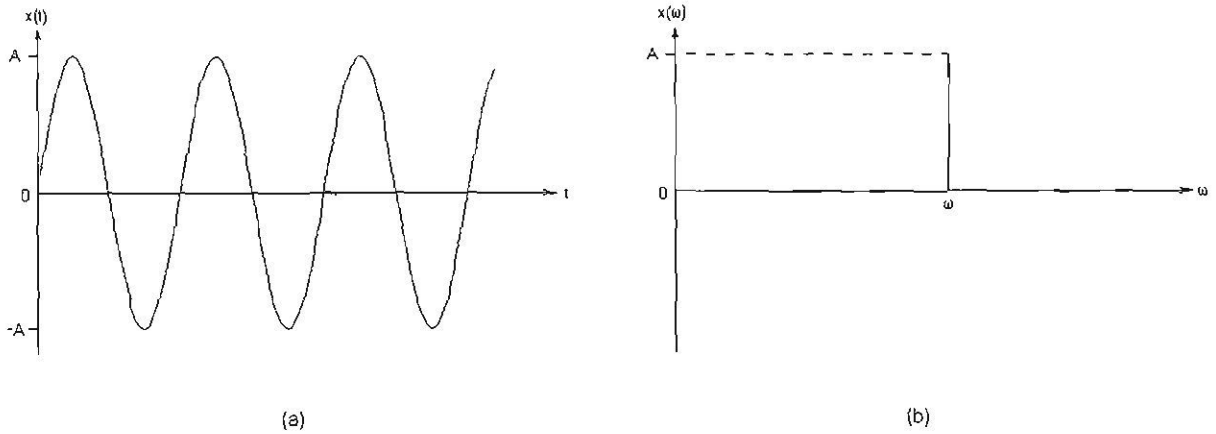


**Figure 2.3 Representation of a function in time and frequency domain (Rao, 2004:57).**

A Fourier integral can represent even nonperiodic functions in either time domain or frequency domain. The Fourier series (Rao, 2004:54) can represent a periodic function $x(t)$ by:

$$x(t) = \frac{a_0}{2} + a_1\cos\omega t + a_2\cos 2\omega t + \cdots + b_1\sin\omega t + b_2\sin 2\omega t + \cdots \qquad (2.4)$$

Here $a_i$ and $b_i$, i=1...n, is the Fourier coefficients. The analyzer computes these spectral coefficients. Modes can be characterized as either rigid body or flexible body modes. All structures have up to six rigid body modes. That is three translational and three rotational modes. Many vibration problems are caused by the excitation of one or more flexible body modes. Fundamental modes (low frequency modes), are given names like that in Figure 2.4. As the frequency gets higher, the appearance become more complex and these modes do not have common names.

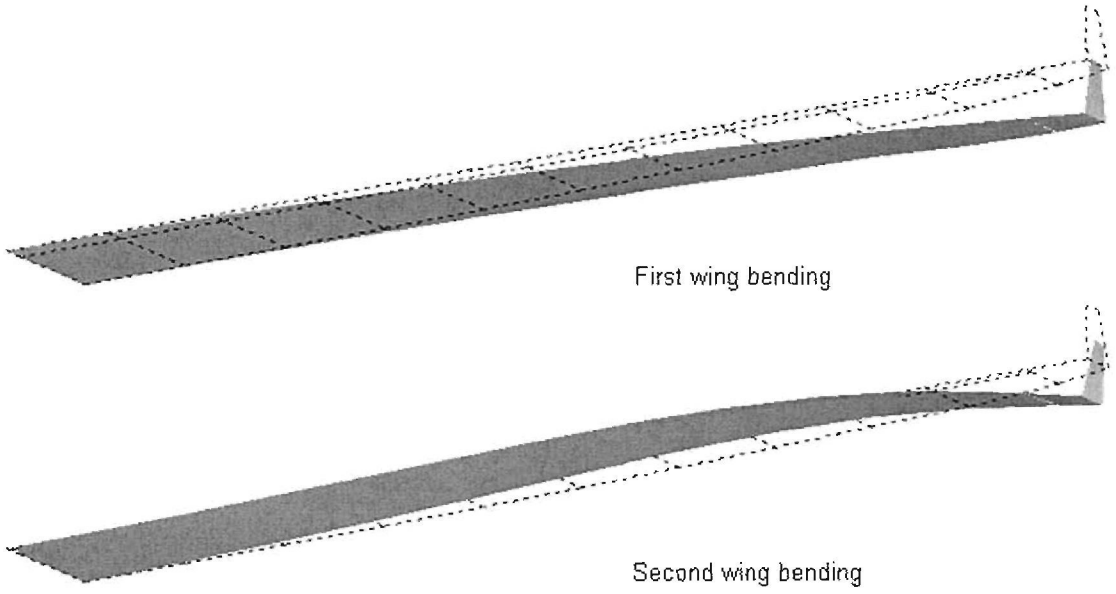


**Figure 2.4 Flexible body modes of a wing.**

The frequency response function (FRF) describes the input-output relationship between two points on a structure as a function of frequency. The FRF is a fundamental measurement that can be use to obtain modal parameters of a structure. A FRF, $H(\omega)$,is defined as the ratio of the Fourier transform of an output response ( $X(\omega)$) divided by the Fourier transform of the input force ( $F(\omega)$), (Richardson & Schwarz, 1999:2):

$$H(\omega)=\frac{X(\omega)}{F(\omega)} \tag{2.5}$$

The FRF and its inverse have a variety of names depending on what response motion is measured. (Acceleration/force) is called inertance or receptance and the inverse thereof is called the dynamic mass. A FRF is a complex valued function of frequency and can be displayed in various formats such as the Nyquist, Nichols, and Bode diagrams.

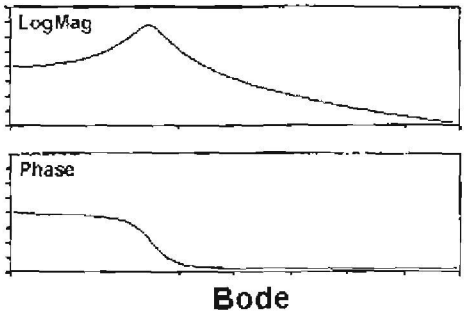


**Figure 2.5 An example of a Bode diagram (Richardson & Schwarz, 1999:2)**

When a vibration test is done with the use of a shaker, the input is fixed and FRFs are measured for multiple outputs. A FRF matrix can be constructed from measurements where columns of the matrix correspond to inputs and rows correspond to outputs. Thus, with a typical shaker test, the elements from a single column of the FRF matrix are measured. With the shaker test, a load cell or impedance head is fixed between the stinger (connected to the shaker) and the structure to measure the excitation force. Accelerometers are fixed to positions on the structure where the outputs will be measured. Commonly modal parameters are identified by curve fitting a set of FRFs. Curve fitting is the process of matching a mathematical expression to a set of empirical data points. There are many curve-fitting methods. For example, modal parameters can be estimated one mode at a time or estimated with multiple modes at a time.

The frequency of a resonance peak in the FRF is used as a modal frequency. Although it is not exactly equal to modal frequency, it is a close approximation. The width of the resonance peak is a measure of the modal damping. The resonance peak should appear at the same frequency and its width be the same for all FRF measurements. From an inertance FRF, the peak values of the imaginary part of the FRF are taken as components of the mode shape.

## 2.4 *Flutter prediction*

Once the dynamic characteristics (mode shapes and modal parameters) have been determined, the prediction of the flutter prediction analysis can begin. The instabilities to investigate, according to CS-22 mentioned in paragraph 2.2, falls under the two fields of aeroelasticity namely, static and dynamic aeroelasticity.

To understand how to predicted and prevent flutter, it should be understand how it develops. The instabilities, the determination of flutter, and the prevention thereof will be discussed in the following paragraphs.

### 2.4.1 Static aeroelasticity

The instabilities, aerofoil divergence and control reversal, is static or steady state aeroelastic instabilities. The effect of elastic deformation on the lift distribution over the lifting surfaces of airplane wings and tails is the central problem in this field. That is because the aerodynamic forces depend critically on the attitude of the body relative to the flow. The affect of elastic

deformation may become so serious that, at high speeds of flight, a wing can become unstable. A control surface can be rendered ineffective or the sense of control can even be reversed.

Dowell et al. (1995:1) uses the so-called typical section to describe divergence. The typical section consists of a rigid flat plate airfoil mounted on a torsional spring attached to a wind tunnel wall (Figure 2.6).

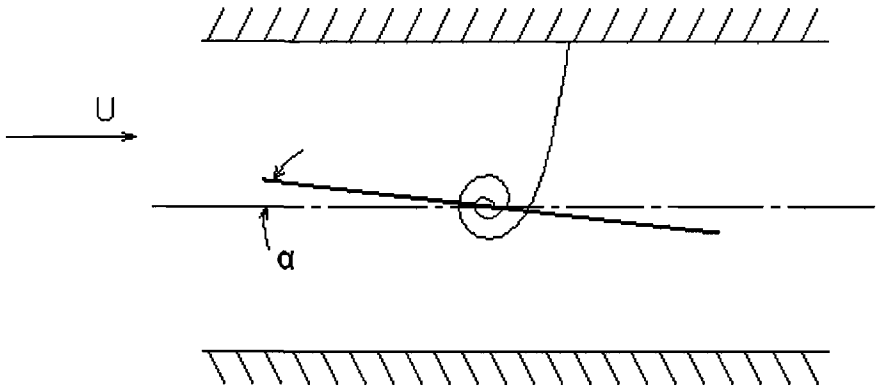


**Figure 2.6 The typical section airfoil (Dowell et al., 1995:3).**

For a low airspeed (or stiff spring), the rotation of the plate would be small. For high flow velocities, the rotation may become so great that the spring is twisted beyond its ultimate strength. The elastic twist, $\alpha_e$, is plotted against the airspeed, $U$ (Figure 2.7). The elastic twist increases rapidly to a point of failure called the divergence airspeed, $U_d$. The curve in Figure 2.7 is also representative of real aircraft wings.

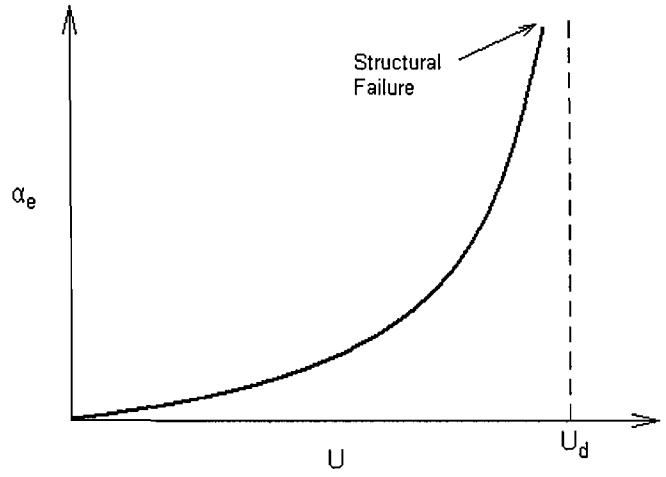


**Figure 2.7 Elastic twist vs. airspeed (Dowel et al., 1995:4).**

According to Fung (1993:82), above this critical speed (divergence speed), an infinitesimal accidental deformation of the wing will lead to a large angle of twist. For modern aircraft, these critical speeds are usually higher than those of flutter or other aeroelastic instabilities are. The divergence speed is often of minor importance but it is a convenient reference quantity for other aeroelastic phenomena.

There exists a critical speed where the ailerons on the wings of an aircraft become completely ineffective. This speed is called the critical aileron-reversal speed. And as an aircraft approach this speed, the aileron control becomes less effective until the aircraft speed is higher than the critical speed. In this case, the aileron control is reversed. For example, when an aileron is displaced downward, lift increases over the wing, lifting the wing tip up. However, above the critical speed, the rolling moment produced by the aileron's downward displacement, moves the wing tip downward.

In addition to the rolling moment, a nose-down aerodynamic pitching moment is also created by the aileron's deflection. When the pitching moment twists the wing, it tends to reduce the lift, and in turn, this reduces the rolling moment. The elastic stiffness of the wing is independent of the flight speed but the aerodynamic force varies with the square of the airspeed. The aileron can thus become ineffective at a critical speed.

### 2.4.2 Dynamic aeroelasticity

Flutter is a dynamic aeroelastic instability and a type of oscillation of the wings and control surfaces of an airplane. Fung (1993:160) gives a good description of this physical phenomenon. Consider a cantilever wing with rigid support in a wind tunnel. It has a small angle of attack with no aileron. With no flow in the wind tunnel, when the wing is made to oscillate, the oscillation is gradually damped. As the flow increases in the tunnel, the damping of an oscillating wing will first increase. If the speed of flow is further increased, a point is reached at which the damping decreases rapidly. Above the critical flutter speed, any small disturbance of the wing can initiate an oscillation with great amplitude. This instability is called flutter.

Experiments have shown that this violent oscillation is self-sustained. The motion of a fluttering cantilever wing has flexural and torsional components. A wing constrained to have no torsional degree of freedom does not flutter. With the flexural degree of freedom

constrained, it can flutter if the angle of attack is near the stalling angle or for special mass distributions and elastic-axis locations.

There are several types of flutter. Dowell et al. (1995:112) gives two types: Merging flutter (bending-torsion flutter) and single-degree-of-freedom flutter. In the former, two (or more) frequencies, in the plot of the real part of the complex frequency versus airspeed (Figure 2.8(a)), will come together near the flutter condition, i.e. where the imaginary part of the complex frequency, $\omega_I$, becomes negative. In single-degree-of-freedom flutter, above some airspeed the positively damped mode becomes negatively damped, i.e. the imaginary part becomes negative. Plotting structural damping versus airspeed, Figure 2.8(b), the onset of flutter is identified where the structural damping coefficient, g, becomes positive.

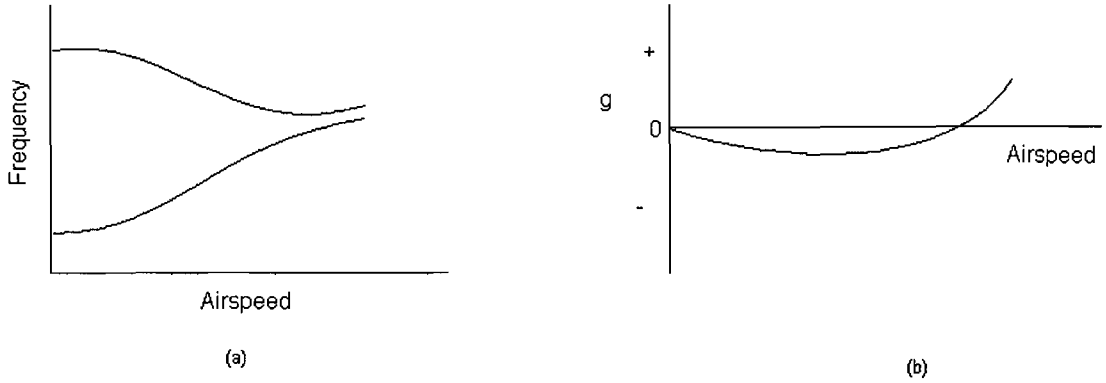


**Figure 2.8 Merging and single-degree-of-freedom flutter (Dowel et al., 1995:112 & 117).**

## 2.4.3 Prediction methods

Hand calculations using tables of aerodynamic coefficients were used to predict flutter during the time of World War II. Since then computer programs were written for the prediction of flutter. However, although computers are extensively used in aeroelastic investigations, actual flight test is also still done to investigate flutter. Both of these two approaches are now discussed.

### 2.4.3.1 Analytical code

A flutter code solves the matrix equation (Hollmann, 1997:69):

$$-\omega^2[GM]+(1+ig_0)[GK]-\omega^2[GQ]\{q\}=0 \qquad (2.6)$$

where,

$\omega$ is frequency,

$g_0$ the inherent structural damping,

$\{q\}$ the complex eigenvector,

$i = \sqrt{-1}$,

[GM] the generalized mass matrix,

[GK] the generalized stiffness matrix,

[GQ] the complex generalized aerodynamic force matrix.

The matrix [GK] contains the squares of the natural frequencies along its diagonal. Equation (2.5) can be written in eigenvalue form as

$$\frac{[GM]+[GQ]}{(1+ig_0)[GK]}\{q\} = \lambda\{Q\} \tag{2.7}$$

with,

$$\lambda = (1+ig)/\omega^2 \tag{2.8}$$

An indirect method, the so-called V-g method is used to compute the flutter velocity. Equation (2.6) is solved for a series of reduced frequency with Mach number and altitude fixed. A number of eigenvalues $\lambda$ (the number of modes used) is produced by each solution. With equation (2.7), the associated values of damping g and $\omega$ are calculated. A plot of $g$ versus V (velocity) gives a set of curves. The critical flutter speed is determined where $g$ changes from negative to positive values (Figure 2.8(b)). To identify what modes are participating most actively in the flutter, a plot of $\omega$ versus V is used. Finally, the Mach number and or altitude are varied until the critical flutter speed matches that implied by the choice of altitude and Mach number.

Another solution method is the p-k-method. In this method, the aerodynamic matrix is represented as springs and dampers. A frequency is estimated, an eigenvalue is found, and this is used in turn to find a new frequency. The advantage is that the convergence is rapid. In addition, the damping values obtained are more representative of the physical damping. This method is chosen over the k-method, which calculated damping is not physical, and can take a lot of execution time.

For calculation of subsonic, unsteady aerodynamics on the lifting surfaces, the doublet-lattice method is used. It is considered one of the best methods for analysing control surface, multiple interfering surfaces and interfering surface-body configurations (Hollmann, 1997:70).

### 2.4.3.2 Flight tests

Like in the early days of flight, flutter flight-testing is still a hazardous test because aircraft is flown close to actual flutter speeds before instabilities can be detected. The development of flight flutter tests started in 1935 by Von Schlippe who conducted the first formal flight flutter test in Germany. His objective was to lessen the risk associated with flutter testing. With his method, a flutter speed could be estimated form sub-critical airspeeds by exciting the structure during flight. Excitation systems are still used today and efforts go into improving it to enhance vibration data and to reduce uncertainty levels in stability estimates. Excitation mechanisms are one of the automated techniques researched to improve the flight flutter test process. Signal analysis of aeroelastic data and robust flutter boundary prediction methods is two other important elements in this research.

Considerable time and money go into flight-testing and researchers are looking at new methods to safely and accurately predict flutter and to reduce costs. Several methods has been developed and evaluated for predicting flutter. Two of these methods are described below.

Damping extrapolation

Damping extrapolation is a data-based method. It relies only on flight data with no consideration of theoretical models. The flight data is used to predict values of modal damping ratios. The onset of flutter is predicted by extrapolating trends of modal damping. This is the most commonly used method (Lind, 2002).

At least one mode's damping becomes zero at the onset of flutter. The variation of modal damping with airspeed is noted and the variation extrapolated to an airspeed at which the damping should become zero. There are however, some difficulties in practice and the extraction and extrapolation of the modal damping present these difficulties. In the former, the low signal-to-noise ratio of flight data may require sophisticated techniques. In the latter, damping can be a highly non-linear function of airspeed.

Flutterometer

The flutterometer is a tool that differs from the approach mention in the above paragraph. It is a model-based approach and uses both flight data and theoretical models to predict where flutter starts. Frequency-domain transfer functions from sensors to excitation are obtained from the flight data and the model used is the corresponding theoretical transfer function. The

formulation of this approach is based on the $\mu$–method analysis. It computes a stability measure that is robust with respect to an uncertainty description.

With the flutterometer, a robust flutter speed is computed at every test point. The first step is to compute an uncertainty description for the model at that flight condition. This is done by noting differences between the theoretical and measured transfer functions. Next, the robust flutter speed is computed. This step is done by applying the $\mu$–method analysis on the theoretical model that contains the uncertainty variations. The flutterometer thus predicts a realistic flutter speed that directly accounts for flight data and is thus more beneficial than theoretical predictions.

### 2.4.4 Prevention methods

According to Fung (1993:160), the oscillatory motion of a fluttering cantilever wing has both flexural and torsional components, as previously mentioned in paragraph 2.4.2. Experiments done on wing flutter revealed several facts, where the above mentioned is one. Another fact is that at the critical speed the steady oscillations are simple harmonic. At all points, the flexural movements are approximately in phase with one another and likewise for the torsional movements, but the flexural and torsional movements are not in phase. In truth, the torsional displacement lags considerably behind the bending. And this motion depends largely on the speed of the air passing the wing.

For purposes to define the way bending and torsion is measured, a reference section of the wing, close to the tip, is chosen. This slice is assumed to move as a rigid body. There exists a reference point in the section called the flexural centre where no twist is produced when a normal bending load is applied and no bending when pure twisting is applied to the section. With this reference point, flexure and torsion is not coupled by elastic forces. When a wing is twisted in still air so that the flexural centre is not moved from equilibrium, and suddenly released, the ensuing motion is not purely torsional. Therefore, when one of the two motions is present, it will tend to induce the other one and the two motions will couple. In general, flexure and torsion are coupled by inertia (Duncan, 1945:19). This coupling is measure by what is called the product of inertia. When masses of the wing is arrange in a way that the product of inertia is zero, the wing is mass-balanced. With such a wing, one motion will not tend to induce the other.

The basic principle in preventing flutter according to Duncan (1945:19) is to eliminate as far as possible the couplings between the motions in the several degrees of freedom. Ideally, these motions must be independent of one another and flutter will then be completely prevented when each of the motions is damped. So, flutter can be prevented when the flexural centre coincidence with the centre of independence (which is a kind of averaged aerodynamic centre of the entire wing) and when the wing is mass balanced about this common centre (see Figure 2.9). In addition, the torsional elastic stiffness of the wing can be made sufficiently large.

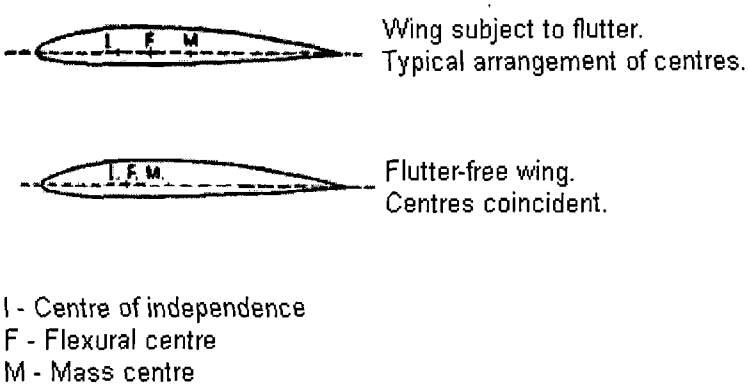


**Figure 2.9 The arrangement of centres for wings subjected to and free from flutter (Duncan, 1945:19)**

## 2.5 Methods overview

As stated earlier, the CS-22 will be used in this study because it is replacing the JAR in Europe. An experimental modal analysis by means of a GVT will be performed. For excitation, a logical choice will be a modal shaker, chosen over an impact hammer. For reasons of availability and cost, MEMS accelerometers will be used on the glider. The theory of determining the dynamic characteristics where given, but this is obviously incorporated into software which will be described in Chapter 3. The flutter prediction will be done by using a software code using the doublet lattice method and the p-k solution method. Flutter flight tests will not be done for it is not within the scope of this study.

## 2.6 Summary

This chapter presented the literature applicable for a flutter analysis for an aircraft. The regulations for such an analysis where stated and the procedures and methods for accomplishing it where given. The procedure that is going to be used in this study is an

experimental modal analysis and a flutter prediction with the use of an analytical code. Information was also given about prediction of flutter with flight-testing and methods for preventing flutter. Although not part of this study, the information could be used as a starting point for a next study.

# 3 MODAL ANALYSIS: GVT

## 3.1 Introduction

This chapter will describe the whole process of preparing the glider for a ground vibration test and setting up the instrumentation. A ground vibration test is a practical way of performing a modal analysis.

A modal analysis is the process of determining the dynamic characteristics of a vibrating system. The dynamic characteristics needed in the flutter analysis are the mode shapes, natural frequencies and damping ratios associated with each of the mode shapes. A modal analysis is performed by using an analytical method or ground vibration test (GVT). Since an analytical approach was taken in the preliminary study by using finite element software, the next step is to do a more accurate prediction of the dynamic characteristics by performing a GVT.

Modal parameters and mode shapes of the JS1 glider were determined by means of a ground vibration test (GVT). Since the university do not have the facilities and all the instrumentation to do a GVT, the services of the Council for Scientific and Industrial Research, CSIR, were used. They do amongst other things aeronautical research development and application. Since 1978, they have analyzed more than 120 different aircraft configurations and aims to meet the needs of the South African Defence Force and aeronautical industry.

## 3.2 Preparation

Before the vibration tests could begin, the sensors had to be attached and connected to the required hardware. A model of the glider had to be created to use in the software and channels set up to correctly read the signals and the direction it measured. This whole preparation process will now be discussed in the following paragraphs.

### 3.2.1 Accelerometer positions

The first thing to determine was the modal data points. It is the positions on the aircraft where the output from the excited structure will be measured and thus where accelerometers will be fixed. Care must be taken not to choose too few points; otherwise, the points will not collect

enough information to accurately predict the mode shape of the structure (see Figure 3.1). The number of points that can be used also depends on the amount of accelerometers that are available and how many channels the hardware and software can process.

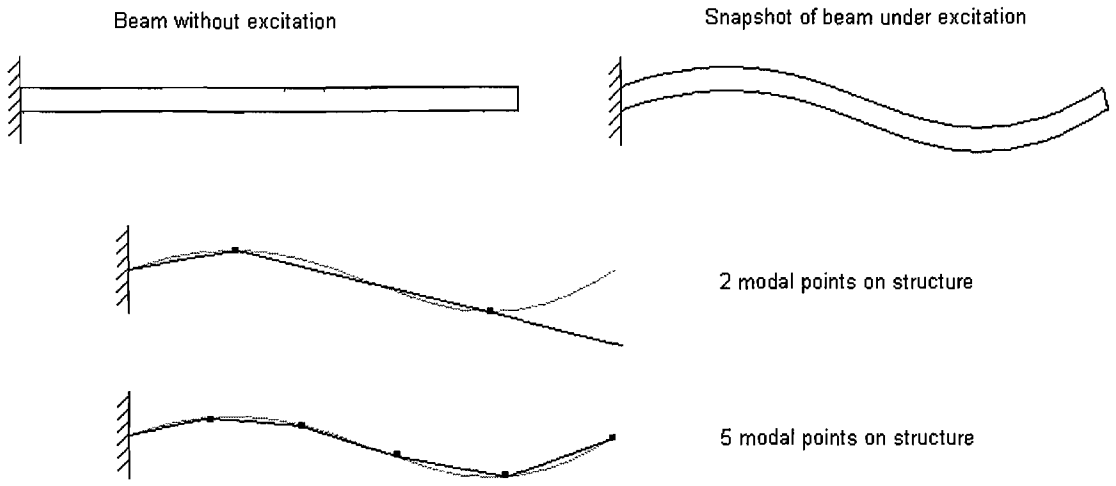


**Figure 3.1 Modal point selection and layout**

The accelerometers available was triaxial and single-axes accelerometers. These accelerometers are so called MEMS (Micro-Electro-Mechanical Systems) accelerometers, which measure acceleration by sensing the change in capacitance. It works very effective for this low g application. The single-axes accelerometers were used on the two wings of the glider while the triaxial accelerometers were used on the rest of the aircraft. The amount of accelerometers on each part of the glider is as follow:

- 5 triaxial accelerometers on the fuselage
- 9 triaxial accelerometers on the fin
- 18 triaxial accelerometers on the tailplane
- 48 single-axes accelerometers on the right wing
- 48 single-axes accelerometers on the left wing

A sketch of the positions is given in the Appendix, page 54. Because displacements on the wing normal to the direction of flight are greater in amplitude than those measured in the plane of the wing, single-axes accelerometers were used on the wing. To measure the in-plane motion of the wings (horizontal movement), accelerometers were fixed to the leading edge of the wing, (Figure 3.2).

Accelerometers were fixed by silicone. The single-axes accelerometers itself was in a silicone housing. It was thought to be the best way of attaching the accelerometers without doing damage to the glider's surface. The problem was that the silicone did not come of easily afterwards. It had to be sanded off and the surface repolished. For following tests, masking tape was attached to a position and then an accelerometer would be glued to the position by silicone. This method work very effectively.

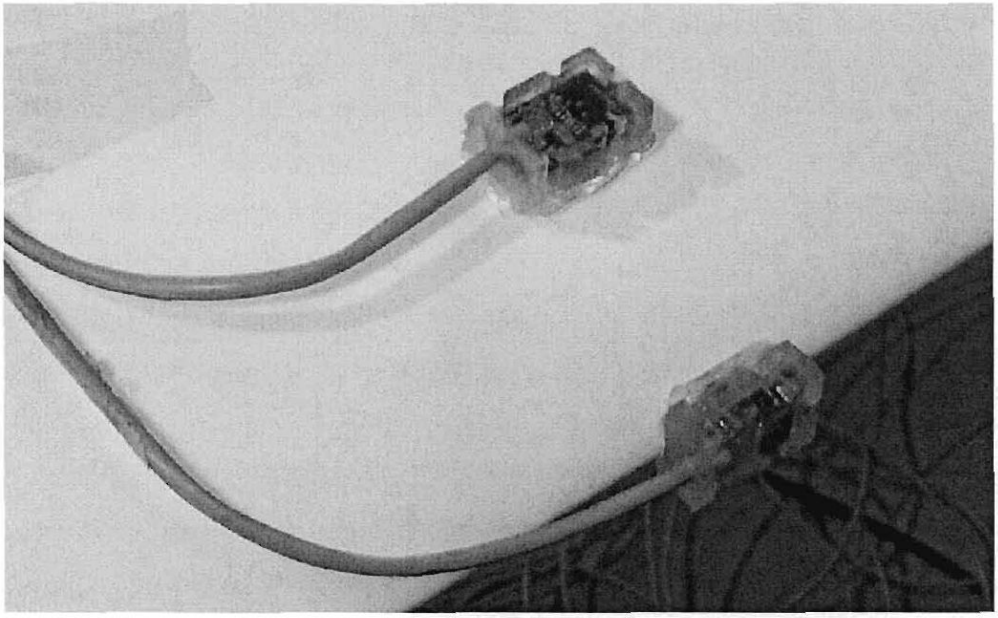

**Figure 3.2 Two single-axes accelerometers near and on the wing leading edge.**

A maximum of 16 accelerometers were connected to a circuit board to which a 12-volt battery were also connected. The purpose of the circuit board was simply to supply the sensors with power and did no processing. Cables connected each of the circuit boards to a simultaneous sampling unit. This unit is used for multichannel spectral analysis and applications that perform transfer function computations. The simultaneous sampling unit were connected to and controlled by a data acquisition processor on a pc.

### 3.2.2 Glider model

A model of the glider was created to visually inspect a mode. Thus, while extracting a mode during a test, the motion of the mode could be observed to determine what type of mode was under investigation.

Flat panels of the wings, fin and tailplane where created from an aerodynamic 3D model of the glider. The panel model of the wing was divided into smaller rectangular panels. The same is

true for the other surfaces. The corners of the panels are the positions where modal data were extracted. The process was thus simply selecting the positions where the modal data would be extracted from and using these points to create the panels for the glider model. Each point's coordinate were taken from the 3D model and entered into the software that was used to create the panel model. Since the fuselage had only five modal points on the one side, it was represented by lines (Figure 3.3).

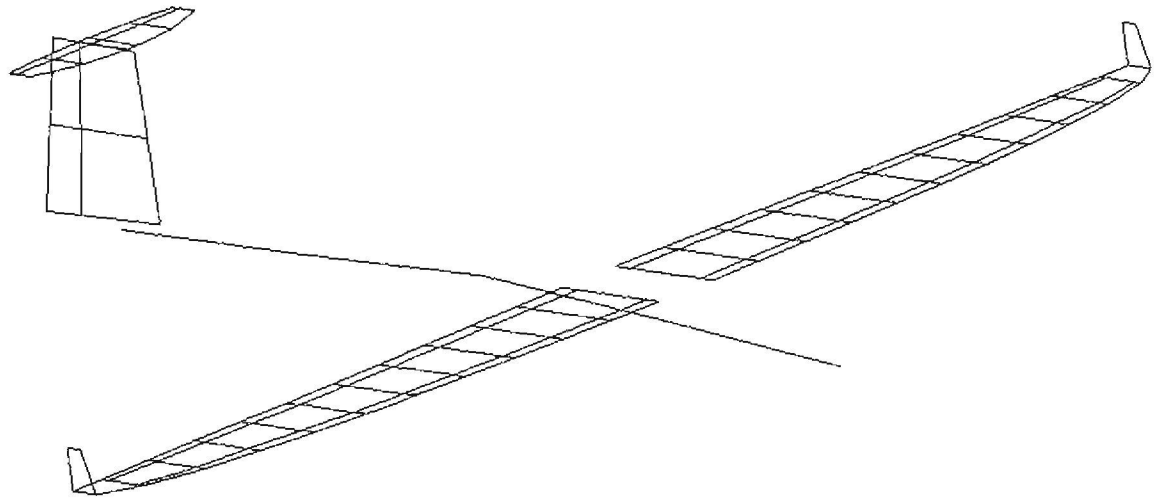

**Figure 3.3 Panel model of glider for determining mode type.**

The wings of the glider curve upwards from inboard to outboard. The panels were created along the wing and then bended downwards to create a horizontal flat panel wing (Figure 3.4). Except for the winglets at the tip of the wing, this was kept vertical. Accelerometers were positioned at such an attitude on the wing to measure the vertical displacement normal to the horizontal and not normal to the real wing. These displacements can then later be rotated with the wing sections (in the panel model) when used in the flutter prediction code.

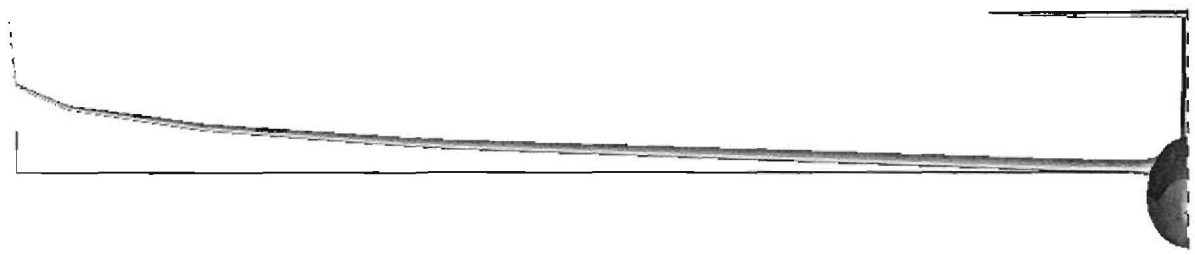

**Figure 3.4 Flat panel wing model versus the real curved wing.**

### 3.2.3 Glider support system

During vibration testing, a structure must be fixed in a way to obtain the desired constraints. The constraints are the boundary conditions and it affects the overall structural characteristics of the system under excitation. When an aircraft flies through the air, it is in a free condition. A free condition means that a structure is floating in space with no attachments to the ground and exhibits rigid body motion at zero frequency (Hewlett Packard, 1997:16). It is thus necessary to simulate this free condition during testing. It is however not physically possible, as a result, a structure must be supported in some manner.

To approximate a free system, a structure can be suspended from very soft elastic chords or be placed on a very soft cushion. In the case of a glider, a suspended option will be the better choice since it would be difficult to place it onto some kind of cushion. The facility at the CSIR where the glider was tested had an overhead crane with 30-ton capacity. Enough capacity to lift a 600 kg (maximum) glider and making the suspended option more realizable.

Therefore, the decision was to suspend the glider with a few springs to the crane. The springs were garage door springs of almost 1 meter in length. A quick test showed that one such spring could carry a load of 180 kg without plastic deformation. With empty water tanks, the glider weighs about 400 kg. With water ballast, it weighs about 600kg. Three springs could thus be put in parallel to carry the glider's weight at 400 kg and four springs could be put in parallel to carry the glider's weight at 600 kg. Why four springs in parallel was not chosen for the 400 kg weight case will be explained shortly.

Given that the structure is supported, the rigid body mode frequencies are not zero. However, the stiffness of the support can be adjusted to obtain frequencies as low as possible. Hewlett Packard (1997:16) gives a rule of thumb that the highest rigid body mode frequency must be less than one tenth that of the first flexible mode. According to another source (Carson et al., 1997:7), the rigid body mode frequencies must be less than a quarter of the first flexible mode. If this criterion is met, the rigid body modes will have negligible effect on the flexible modes.

The natural frequency of a simple spring-mass system in vertical position and the spring constant is given respectively by:

$$\omega_n = \left(\frac{k}{m}\right)^{1/2} \tag{3.1}$$

and

$$k = \frac{mg}{\delta_{st}} \tag{3.2}$$

Here $m$ is the mass in the system and $g$ the standard gravity. The spring constant of the garage spring were determined from the data obtained from the quick test and was calculated as 3087 N/m. The load the spring should carry governed the quantity of springs in parallel. Thus, three springs in parallel will have an effective spring constant of 9260 N/m and carry the load of 400 kg. Equivalently, four springs will have a constant of 12347 N/m carrying the load of 600 kg. By coupling each of these pairs of springs in series, the effective spring value for each load case can be manipulated to obtain a natural frequency that comply with the rules given in the previous paragraph. However, the amount of pairs put in series is also governed, in this case, by the distance available from the glider to the roof.

Using equations (3.1) and (3.2), the resonant frequency of the spring (spring combinations) and mass (mass of glider) system could be determined. Dividing this frequency with the lowest bending frequency, determined from the finite element model in the preliminary study (1.888 Hz), gives the ratio that could be compared by the rules stated in this section. Table 1 shows the combinations of springs and the ratios it gives. The last two columns also give the ratios calculated with the true lowest bending frequencies of each load case. The spring combinations could only be chosen with the preliminary data. The bold lines indicate the chosen combinations. Coming back to the reason why in the 400 kg load case the four springs in parallel option was not used, is in column six. With three springs, the ratios are better than with four springs in parallel.

**Table 1: Spring combinations used to suspend the glider.**

| Load case | Springs in parallel (a pair) | Pairs in series | Effective spring constant [N/m] | $\omega_n$ [Hz] | $\omega_n$ / 1.888 (prel.) (600 kg) | $\omega_n$ / 2.403 (GVT) (400 kg) | $\omega_n$ / 2.045 (GVT) (600 kg) |
|---|---|---|---|---|---|---|---|
| 1 (400 kg) | 3 | 1 | 9260 | 0.766 | 0.406 | 0.319 | - |
| | **3** | **2** | **4630** | **0.541** | **0.287** | **0.225** | - |
| | *4* | *1* | *12347* | *0.884* | *0.468* | *0.368* | - |
| | *4* | 2 | *6173* | *0.625* | *0.331* | *0.260* | - |
| 2 (600 kg) | 4 | 1 | 12347 | 0.722 | 0.382 | - | 0.353 |
| | **4** | **2** | **6173** | **0.511** | **0.270** | - | **0.250** |

Although the preliminary ratios from the combinations chosen, are not less than a quarter as indicated by Carson et al. (1997:7), another source (Van Zyl, 2007) who is an expert in the

field indicated that the rigid body mode frequencies must be less than half of that of the first flexible mode. This is true in the preliminary determination, but with the actual testing, the ratios became better and were equal to and less than a quarter as indicated by the former source.

The spring system was connected to the overhead crane and glider by strong straps and shackles. Steel cables were loosely put through the springs as a safety precaution. A picture of the setup is given in Figure 3.5. The weight of the glider had also to reflect the true weight and thus the mass of a pilot was taken as 100kg. 20 kg sand backs were used to make up this weight and were put onto the seat in the cockpit.

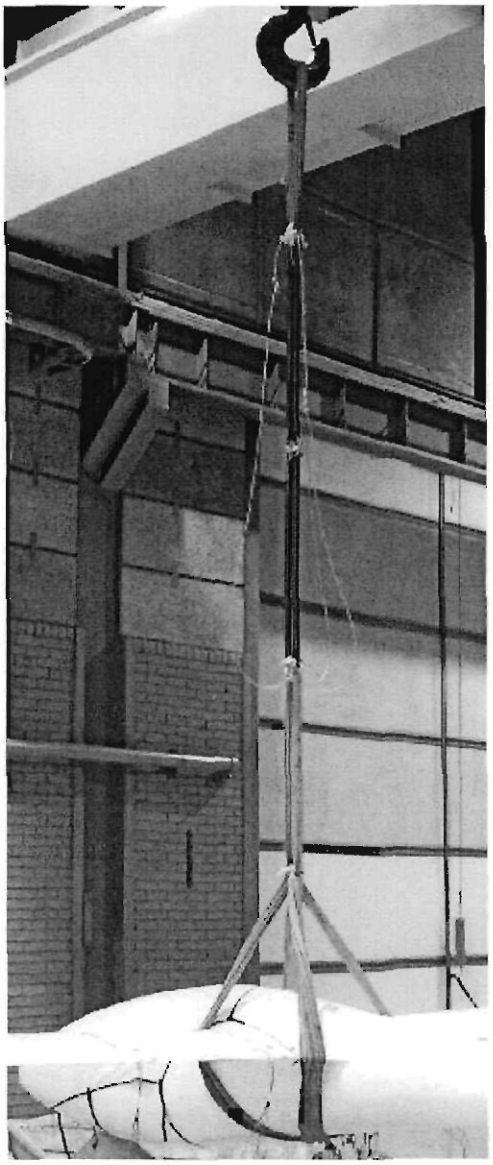

**Figure 3.5 Spring support system simulating a free boundary condition.**

### 3.2.4 Excitation position

To excite the glider, an electrodynamic shaker was used. Excitation positions were on the outboard part of the wing, near the tip of the tailplane and at the back of the fuselage. The positions and number of shakers used depended on the specific mode under investigation.

First just one shaker is used near the tip of the wing. If a specific mode cannot be extracted entirely, another one is used on the opposite side of the wing or on the back of the plane. For example, an anti-symmetric mode can be clearly excited by two shakers on opposite sides of the wing, shaking out of phase. The response of all the accelerometers is graphically displayed by a bar graph, each bar representing a sensor. The magnitude and phase of the response are displayed as two separate bar graphs. At a natural frequency, all of the sensor's phase should become zero. This is not always possible to obtain. However, one tries to close the phase part of the response as far as possible. In addition, this magnitude and phase response of the sensors is used to determine if another shaker is needed and approximately where to put it on the glider. For example, when only one shaker is used on a specific position and the phase of another part of the glider's response does not become zero, another shaker is probably necessary at that position.

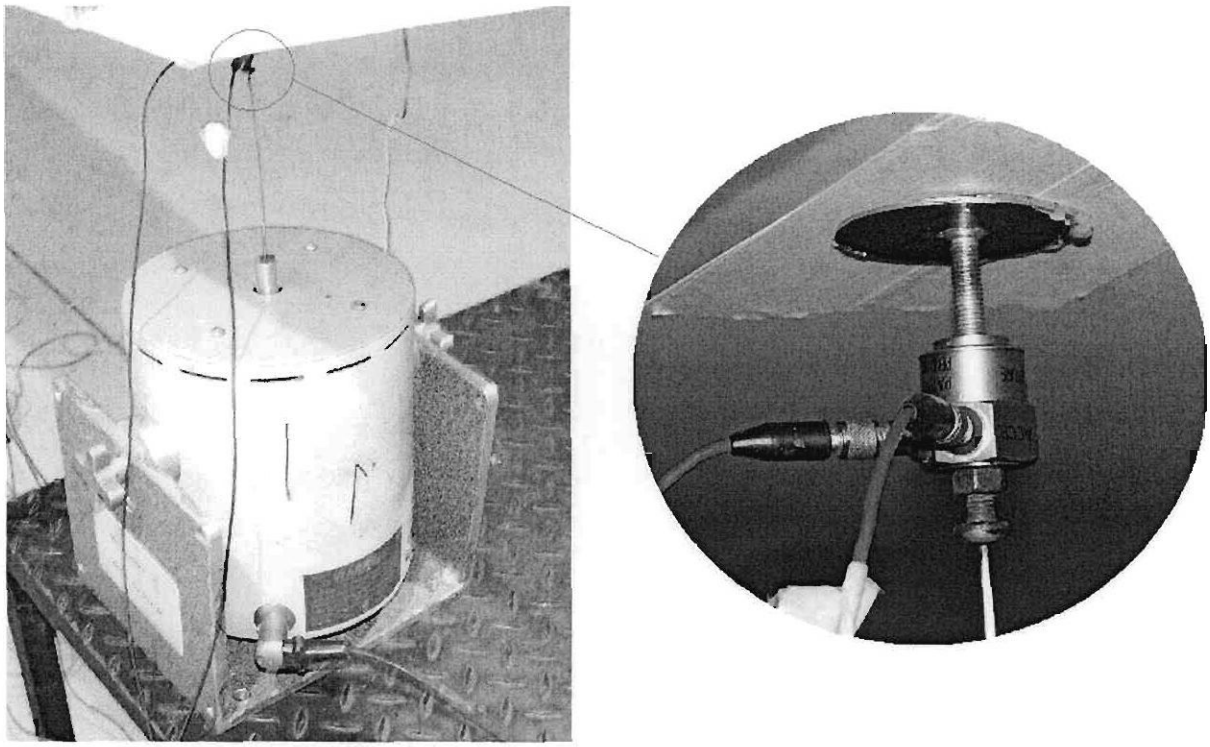

**Figure 3.6 Electrodynamic shaker, stinger, transducer and small plate used to excite the glider.**

To shake the glider, the shaker must be attached to the structure in some way. As described in paragraph 2.3.2.1, a stinger is attached to the shaker and a force transducer attached to the tip of the stinger. The transducer is then screwed onto a small plate, which is glued to the glider surface. Again, care must be taken not to damage the surface. Thus, masking tape was first put on the shaker position before the small plate was glued to the position using hot glue. When the shaker had to be moved to a new shaking position, the masking tape and plate could simply be pulled off without any damage to the glider's surface. Figure 3.6 shows this clearly.

## *3.3 Ground vibration test*

After all the instrumentation was set up, the vibration testing could begin. All the instrumentation and hardware were connected to a personal computer. From the pc the excitation could be controlled, response measured and calculations done. Personnel at the CSIR programmed the software code used during the testing. The window that all the controls were on had the following options:

- Analog to digital on/off button.
- Digital to analog on/off button.
- Frequency button to change the exciting frequency.
- Force or velocity button to change the exciter output type.
- Exciter on/off button with input for force or velocity magnitude. There were four of these options so that four shakers could be attached.
- Graph window for each exciter option with real and imaginary axes showing the force and velocity lines.
- Complex power graph window (Cartesian coordinate system) with real and imaginary parts along the axes.
- Accelerometer response bar graph showing the real and imaginary parts as bars.

The procedure of finding and extracting modes and the dynamic characteristics is discussed in the following paragraphs. First, the configurations for which the tests were done are now discussed.

### 3.3.1 Glider configurations

A glider or sailplane uses thermals (a column of rising hot air) to gain altitude once it is in the air. A glider must be able to fly at high speed between these sources of lift. By adding water in

the wings of the glider, although making it heavier, it also gives a better high-speed performance to the aircraft for moving between thermals. When the weather is such that climbing in the thermals becomes difficult, the water ballast is simply dumped.

This condition of water and no water presents two cases of glider configuration. In the preliminary study, the weight of an engine was included in the analysis. However, this is an option to be added in the future and no engine was thus installed into the prototype glider. Table 2 gives the two configurations of the glider the ground vibration test was done for. The flutter analysis was thus done with data obtained for these two configurations.

**Table 2: Glider configurations.**

| Configuration | Glider components | | | | Weight [kg] |
|---|---|---|---|---|---|
| 1 | Fuselage | Wings | Tailplane | | 400 |
| 2 | Fuselage | Wings | Tailplane | Water ballast | 600 |

### 3.3.2 Excitation

An electrodynamic shaker typically used in a GVT consists out of an electrical conducting coil placed in a permanent magnet (Figure 3.7). The magnet is the body of the exciter. As current passes through the coil, a force is produced on the coil and it accelerates the component connected to the coil. The stinger, used to connect the exciter and the structure being excited, is connected to the coil.

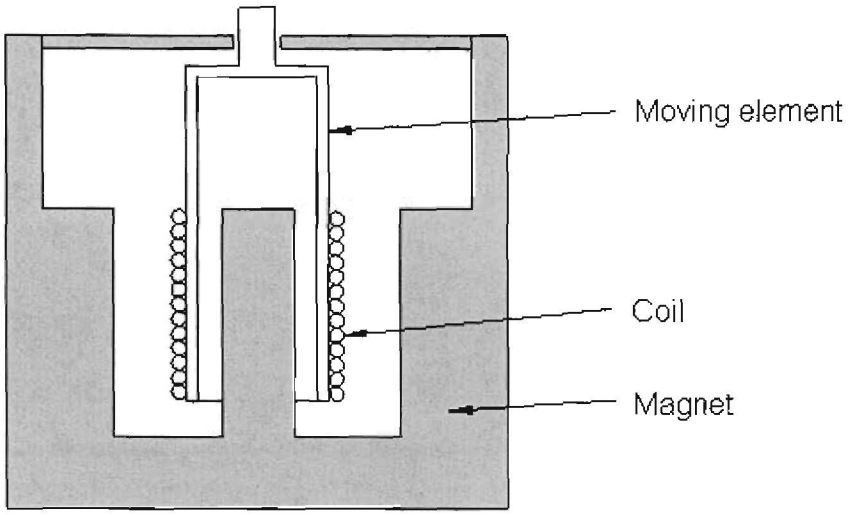


**Figure 3.7 Basic idea behind an electrodynamic shaker (Rao, 2004:763).**

A current harmonically varying with time, passing through the coil. will produce a force which also varies harmonically. In the GVT conducted in this study. a sine-dwell vibration was used. The structure is thus excited to vibrate in phase. In this way. modes can be isolated.

### 3.3.3 Resonant frequencies

To get a clear picture of where the natural frequencies lie, a frequency scan is done. The frequency scan scanned from 1 Hz to 32 Hz changing the frequency in increments specified by the user. When the scan is done, a graph of the amplitude and phase parts of the transfer function is plotted against frequency (Figure 3.8). It takes a few frequency scans with different excitation positions to identify the several natural frequencies that may lie in the frequency range. In Figure 3.8, where the phase turns 180° (from positive to negative) one could expect a natural frequency. The amplitude part could confirm this with a peak. Where the graph is not clear, a scan can be done on a smaller range in the region of the vague area.

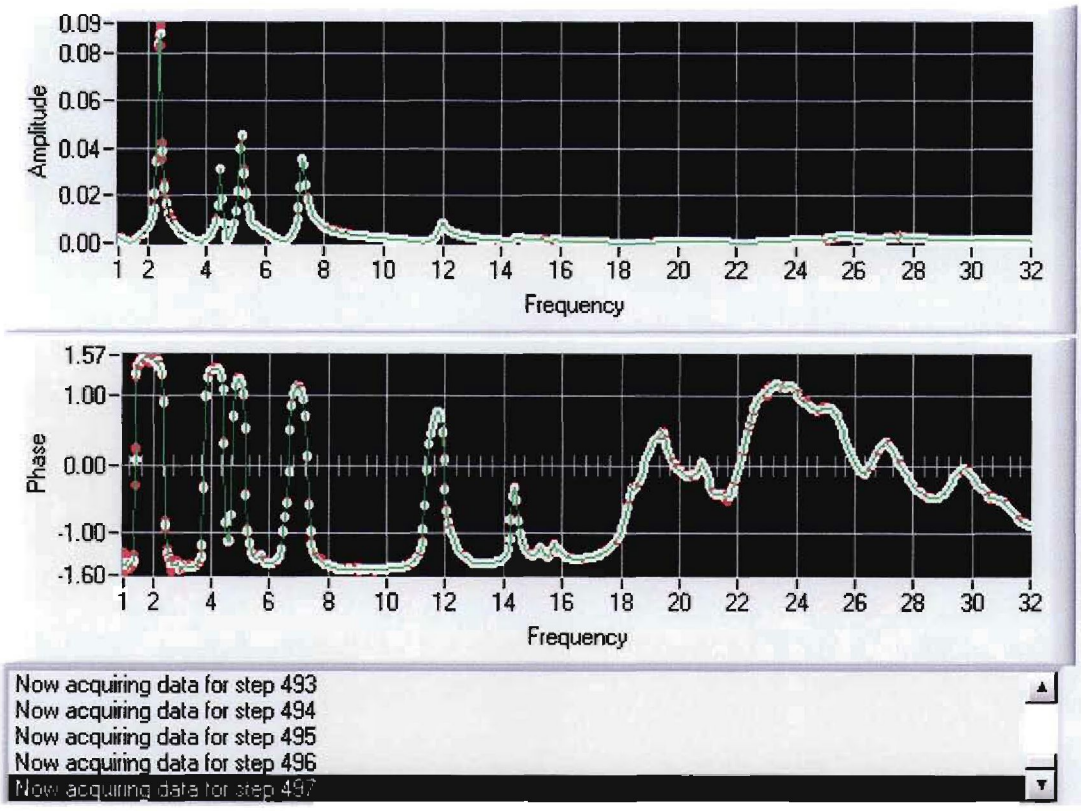


**Figure 3.8 A transfer function of the glider with excitation near wing tip.**

With the approximate natural frequencies identified, the frequency can be manually changed around the natural frequency target. With this procedure, one first tries to get the complex

power to be real with a zero imaginary part (see paragraph 3.3.4 for explanation of complex power method). Normally this is done by changing the frequency down to lower the imaginary part's value if the complex power line lies in the first quadrant of the Cartesian coordinate system. Alternatively, changing the frequency up when the complex power line lies in the fourth quadrant. At the same time, the force and velocity vectors of one exciter are also shown on a Cartesian coordinate system. The force and velocity vectors must also have only a real part and thus be in phase. All this is done by changing the frequency and changing the value of the force or velocity input and watching the response of the system. Only a force input or a velocity input can be used to control the exciter. The testing showed that a velocity input work well for lower frequencies (up to about 10 Hz) and a force input for higher frequencies. That is, when a velocity input is used at the lower frequencies the structure settled faster than with a force input. A structure settling percentage is available to show the user if it is necessary to wait before a change could be make, for example change the frequency. The structure should settle first to show the effect of the changes made to the system, before further changes is made.

When more than one shaker is used, force and velocity vectors of each, together with the values of input force or velocity and the complex power, should be change to get the required results as explained in the above paragraph. In addition to this, the phase response of the accelerometers should also be as close to zero as possible. As mentioned earlier, it is not always possible to get the phase completely zero. The best phase response for the desired requirements in the above paragraph is thus sought.

### 3.3.4 Mode extraction

When a natural frequency is found by using the procedure described in paragraph 3.3.3, a mode can then be extracted. By extraction is meant that the natural frequency, modal damping, modal mass, and the displacements at all the accelerometer positions is calculated and written to an output file. Before a mode is extracted, the model created to visualize the motion of the particular mode can be used to determine the kind of mode shape. Figure 3.9 shows a mode shape and clearly, it is symmetric wing torsion.

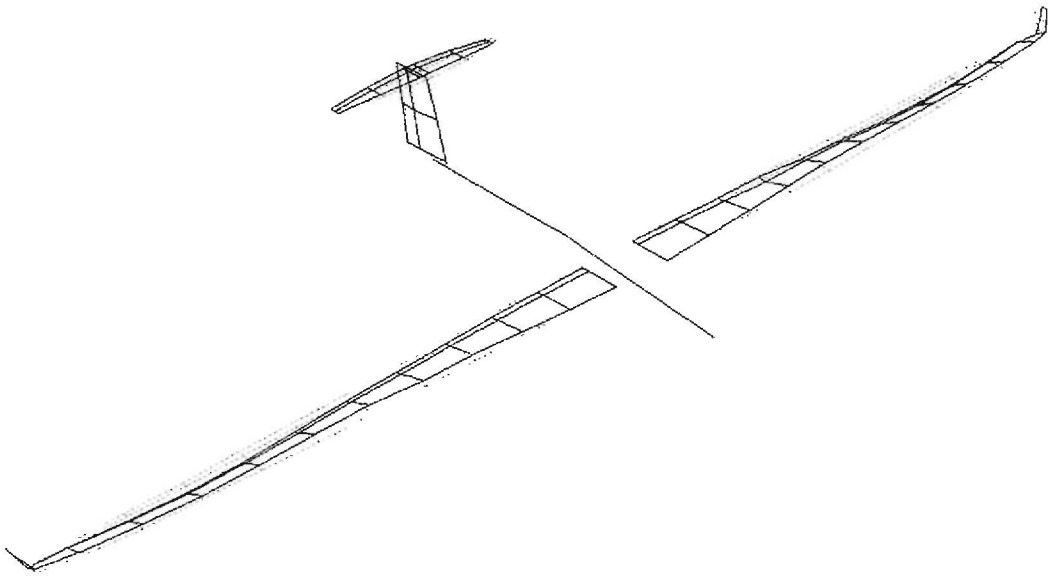

**Figure 3.9 Symmetric wing torsion mode animated by the software.**

The complex power method is used to extract the modal parameters. The complex power is recorded over a small frequency range around the resonant frequency. The software scans through this range in increments, again chosen by the user. The complex power is the product of the excitation force and the conjugate of the resulting velocity. For force feedback (force input), a force is prescribed and defined to be real. With response feedback, a prescribed velocity (velocity input) is produced by the excitation force and defined to be real. For force feedback the complex power is

$$P = \frac{F^2\left[\omega^2 C - i\omega\left(K - \omega^2 M\right)\right]}{\left(K - \omega^2 M\right) + \omega^2 C^2} \tag{3.3}$$

And for response feedback the complex power is

$$P = \dot{x}^2\left[C - i\frac{K - \omega^2 M}{\omega}\right] \tag{3.4}$$

with $F$, $C$, $K$ and $M$ the harmonic excitation force, system damping, system stiffness and system mass respectively. $\omega$ is the frequency and $\dot{x}$ the velocity. For force feedback, at the resonant frequency, $\omega = \omega_n$, the complex power is

$$P\big|_{\omega=\omega_n} = \frac{F^2}{C} \tag{3.5}$$

The real part is thus a maximum and the imaginary part zero at resonance. When using response feedback, the complex power at the resonant frequency is

$$P\big|_{\omega=\omega_n} = \dot{x}^2 C \tag{3.6}$$

The real part is thus constant and the imaginary part zero at resonance. The maximum value of the real part and root and slope of the imaginary part is determined by curve fitting. Polynomials are fitted separately to the real and imaginary parts. Solving these polynomials gives the maximum value, root, and slope. The natural frequency, $\omega_n$, is determined from the root of the imaginary part only.

When the extraction is done, two graphs are then plotted; the real and imaginary parts of the complex power against frequency (Figure 3.10). During the micro scan, the software takes a few measurements per frequency interval and then an average is calculated (light dots in Figure 3.10). A line is then fit through the data of the real part of the power and if it resembles a parabolic line, the data extracted is most likely good. By good is meant that the mode under investigation is well isolated.

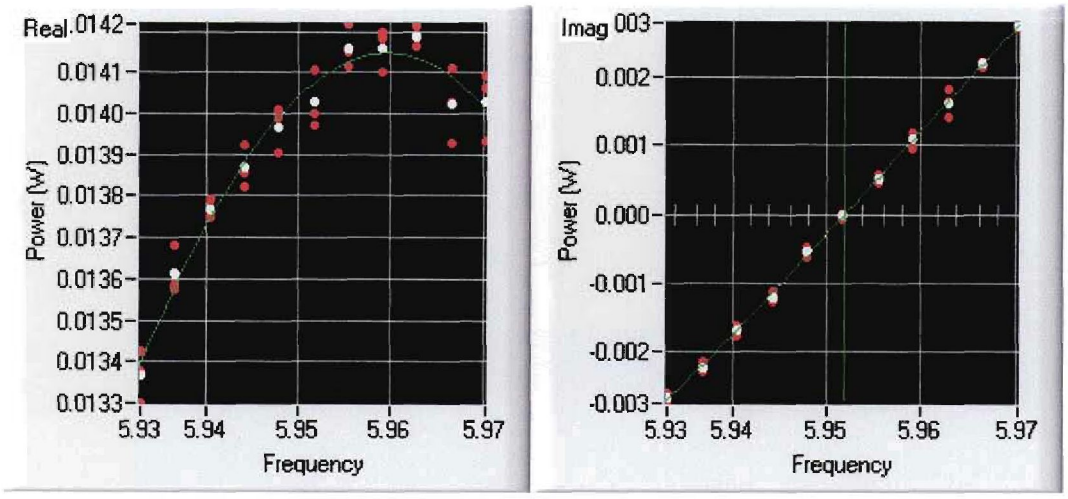


**Figure 3.10 Real and imaginary parts of complex power recorded during micro scan.**

## 3.4 Results

The results of interest, the natural frequencies, modal damping and mode shapes of each mode, were written to an output text file as mentioned in the preceding paragraph. The appropriate values could just be extracted from this file and copied into the input file for the flutter analysis program.

### 3.4.1 GVT results

In the first GVT, the glider was tested only without water ballast in the wings and 16 modes where found. When the second GVT was conducted, 17 modes were found with no water ballast and 19 modes were found with water ballast in the wings. The table below gives a summary of the modes found with their resonant frequencies.

**Table 3: Modes found in ground vibration test between 1 Hz and 32 Hz.**

| Mode description | 1st GVT (no water) | 2nd GVT (no water) | 2nd GVT (water) |
|---|---|---|---|
| | Frequency [Hz] | Frequency [Hz] | Frequency [Hz] |
| 1st Symmetric wing bending | 2.403 | 2.403 | 2.045 |
| 2nd Symmetric wing bending | 7.263 | 7.336 | 5.952 |
| 3rd Symmetric wing bending | 25.99 | 25.327 | 12.397 |
| 4th Symmetric wing bending | - | - | 19.715 |
| Symmetric wing torsion | 27.774 | 28.056 | 16.298 |
| Symmetric wing in-plane bending | 6.361 | 6.547 | 5.358 |
| Symmetric *unknown* | - | - | 21.77 |
| | | | |
| 1st Anti-symmetric wing bending | 5.154 | 5.201 | 3.97 |
| 2nd Anti-symmetric wing bending | 11.903 | 12.082 | 9.409 |
| 3rd Anti-symmetric wing bending | 30.259 | 29.838 | 16.668 |
| 4th Anti-symmetric wing bending | - | - | 26.354 |
| Anti-symmetric wing torsion | 24.249 | 26.125 | 19.087 |
| Anti-symmetric *unknown* | - | 24.117 | - |
| | | | |
| Fuselage vertical bending | 11.979 | 11.821 | 10.955 |
| Fuselage horizontal bending | 19.563 | 19.179 | 17.586 |
| Fuselage torsion | 4.47 | 4.47 | 4.549 |
| | | | |
| Fin torsion | 12.444 | 12.601 | 11.998 |
| | | | |
| Stabilizer roll | 8.747 | 8.703 | 8.226 |
| Stabilizer vs. fin bending | 14.587 | 14.539 | 13.41 |
| Stabilizer symmetric bending | 21.486 | 21.162 | 21.139 |

The frequencies of the first and second tests with no water ballast is about the same, and should be, for there were no changes made to the glider during the time between the two tests. With water ballast in the wings, logically the mass of the glider is increased. This has the effect that the natural or resonant frequency of a mode will decrease. This can be seen in the above table, except for the fuselage torsion mode.

In the second GVT, one new mode was identified at 24.16 Hz. It is an anti-symmetric torsional mode. With water in the wings, two extra modes were found in the 1 Hz – 32 Hz range: the fourth symmetric and fourth anti-symmetric mode. One unidentified symmetric mode was also found with water in the wings at 21.77 Hz. Its mode shape looks like a symmetric torsional mode.

### 3.4.2 Comparisons

In the preliminary flutter analysis study a finite element model of the glider were created. With this model, the natural frequencies and mode shapes were predicted. These results are compared with those determined in the GVT in Table 4 below.

**Table 4: Comparison of natural frequencies with the preliminary study.**

| Mode description | Preliminary study (no water) | 2nd GVT (no water) | Preliminary study (water) | 2nd GVT (water) |
|---|---|---|---|---|
| | Frequency [Hz] | Frequency [Hz] | Frequency [Hz] | Frequency [Hz] |
| 1st Symmetric wing bending | 4.024 | 2.403 | 1.888 | 2.045 |
| 2nd Symmetric wing bending | 11.135 | 7.336 | 6.048 | 5.952 |
| 3rd Symmetric wing bending | 18.28 | 25.327 | 12.119 | 12.397 |
| 1st Anti-symmetric wing bending | 3.837 | 5.201 | 3.043 | 3.97 |
| 2nd Anti-symmetric wing bending | 9.684 | 12.082 | 7.697 | 9.409 |
| Wing torsion (Preliminary) | 23.856 | - | 14.056 | - |
| Symmetric wing torsion (GVT) | - | 28.056 | - | 16.298 |
| Anti-symmetric wing torsion (GVT) | - | 26.125 | - | 19.087 |
| (Anti-sym.) Stabilizer vs. fin bending | 18.473 | 14.539 | - | 13.41 |
| Stabilizer symmetric bending | 19.213 | 21.162 | - | 21.139 |

The complete finite element model consisted of a detailed wing and a tailplane section, while the fuselage was sub structured (De Bruyn, 2004:39). The correct stiffness of components such as the water tank and other minor components were not included in the model. The

natural frequencies of these components were thus regarded as non-relevant. Looking at the first two columns of Table 4 above, the no-water wing bending results do not compare very well. This may possibly be because the stiffness of certain minor components was omitted. However, the water wing bending results compare better.

From the preliminary study results, wing torsion was given at 23.856 Hz and 14.056 Hz without water ballast and with water ballast respectively. Nowhere was it indicated if this was symmetric or anti-symmetric torsion. Comparing it with the GVT results, the 23.586 Hz wing torsion relate to the 26.125 Hz anti-symmetric torsion and the 14.056 Hz wing torsion to the 16.298 Hz symmetric torsion.

Again, with the stabilizer results from the preliminary study, it was not indicated if it where calculated with or without water in the wings. Since the preliminary study, the tailplane has been redesigned. Taking that into account, the preliminary symmetric bending results compare well with the GVT results. In addition, the anti-symmetric results do not compare that bad either.

The purpose of the preliminary study was to provide a first theoretical flutter report. It is very difficult to produce an exact and detailed finite element model. Assumptions made and minor components left out could be some of the reasons that the results do not match very good. It could also be because some changes were made to the glider.

## *3.5 Summary*

A modal analysis of the JS1 glider was done by performing a ground vibration test. The glider was suspended from a system of springs and straps to simulate a flying condition. A number of sensors were used to accurately record the dynamic characteristics of the structure. Several modes were identified in the range 1 Hz to 32 Hz and the modal parameters and mode shapes of each were extracted.

Two configurations of the glider were tested. Both are conditions in which the glider could be during flight. That is, with and without water ballast in the wings, presenting the two weight conditions: 400 kg and 600 kg. For both of these configurations a set of modes were identified. Modes of wing bending and stabilizer, fin and fuselage modes were found.

Results were not consistent with those found with the finite element model during the preliminary study. Reasons could be that changes could have been made to the glider after the preliminary study.

# 4 FLUTTER ANALYSIS

## 4.1 Introduction

The flutter prediction is the last step of the whole flutter analysis in this study. An experimental flutter prediction by flight-testing would be the last step of clearing an aircraft of flutter, but this is not the focus of this study. With the modal parameters and mode shapes determined in the ground vibration test, the modal data can now be used by the computer code SAF (Subsonic Aerodynamic Flutter) to predict the critical flutter speed of the JS1 glider. SAF is also used by Aircraft Designs Inc. for flutter predictions of aircraft and is quoted to be one of the best programs for aircraft flutter analysis. SAF uses the doublet lattice method to analyze multiple surfaces and is considered by Hollmann (1997:70) and Wilkinson (as quoted by de Bruyn, 2004:44) as the best method for the speed range of the JS1. SAF also provides a choice between the k and p-k flutter solution methods, where the latter is the better option.

The results produced by SAF are presented in graphs of damping and frequency, versus airspeed. Airspeed can be plotted in either true airspeed or equivalent airspeed. Using the graphs, flutter can be identified where the damping graph (having negative values at first) crosses the zero line and becomes positive. Flutter can also be identified by frequency graphs converging. At the area where the two graphs form a bottleneck, flutter can be expected. If a flutter speed is found, a table is also given with the exact speed, damping, and frequency values.

The design diving speed, $V_D$, for the JS1 glider is 324 km/h. According to the requirements mentioned in the paragraph 2.2, flutter clearance must be shown for speeds up to 388.8 km/h, or 210 knots (1.2 $V_D$). This chapter will describe the preparation for creating an input file for the flutter code followed by a discussion of the results obtained.

## 4.2 Preparation

A text input file is created with all the necessary information. SAF uses this text file to conduct the flutter analysis. The information includes the modal data extracted form the GVT. It also includes a definition of the configuration of the glider. A complete model of the glider can be used, but this is not normally done, since the model can become very large and difficult to handle, with this specific code (Hollmann, 1997:21). It would be ideal to use a complete

model, since the airflow in the wake of the wing would influence the flow over the tail. In the glider's case, it was thought that it would not have such a big influence. Other settings needed in the calculations of the analysis are also included in the input file. Symmetric and anti-symmetric mode data are not used in the same file. Separate input files for each is generated. The next paragraph will describe the creation of the glider model used in the input file.

### 4.2.1 Panel model

A wing is defined as a panel. If the wing is simple, a single panel is used, and for shapes that are more complex the wing is divided into several panels. The centre line of the fuselage is usually taken as the global x-axis. The corners of the panels are then defined from the x-axis. The panels must have four corners. The two sides of a panel that run cord wise must be parallel to the x-axis. The panels are thus trapeziums. Figure 4.1 shows a panel model for the wing of the JS1 glider. Note that the control surface on the wing can also be modelled as panels.

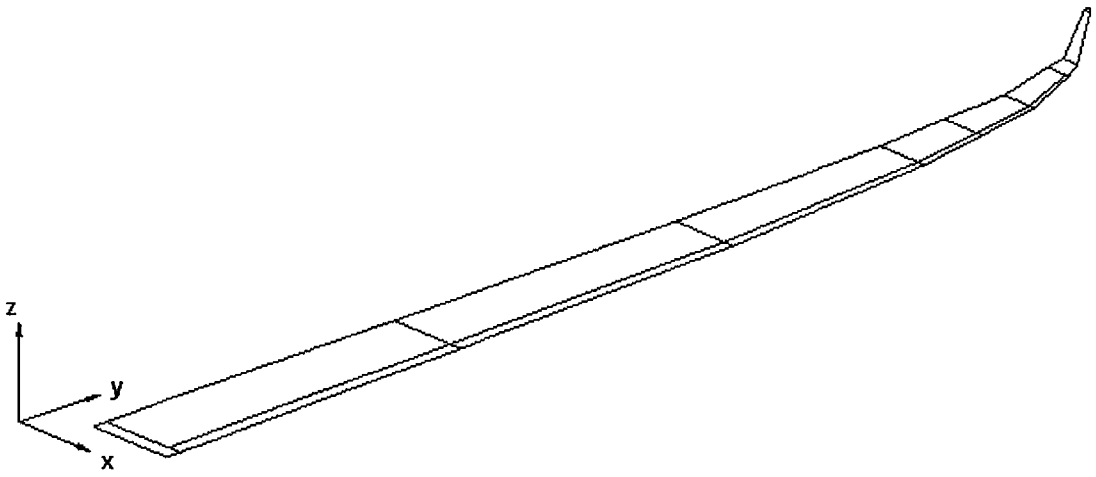


**Figure 4.1 Panel model of the JS1 wing.**

The surfaces that were analyzed and the amount of panels of each are:

- Wing – 15 panels
- Tailplane – 9 panels
- Fin – 2 panels

Each panel were then further divided into doublet lattice elements. These elements are used by SAF to calculate the interaction between the free stream and aircraft structure. As the panels are trapeziums, so are the elements also. The elements are created such that the

element aspect ratio is between one and two. Figure 4.2 shows the part of the wing divided into elements.

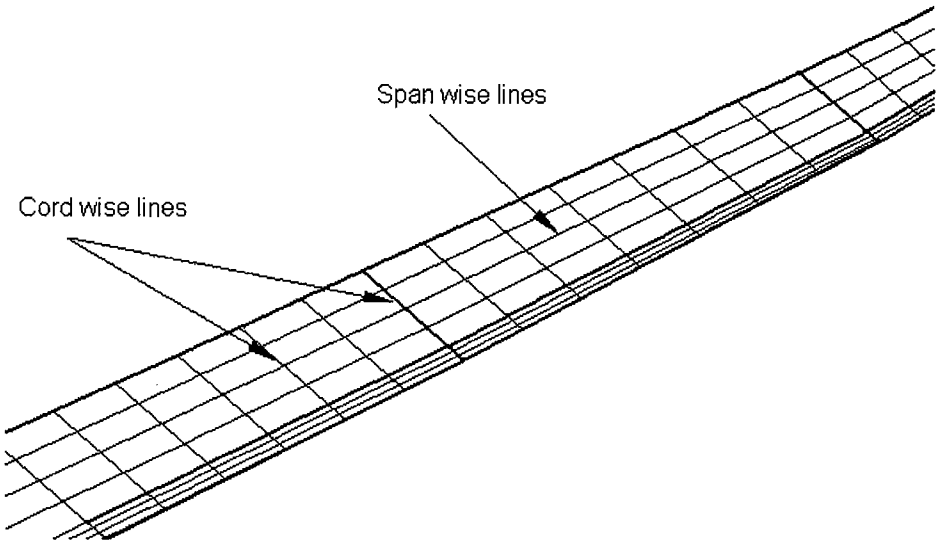


**Figure 4.2 Panels divided in doublet lattice elements.**

### 4.2.2 Modal points

With the panels and elements of the model defined, a definition of where the modal point positions are could now be done. A requirement for SAF is that the modal points must be positioned in a straight span wise line like that in Figure 4.3.

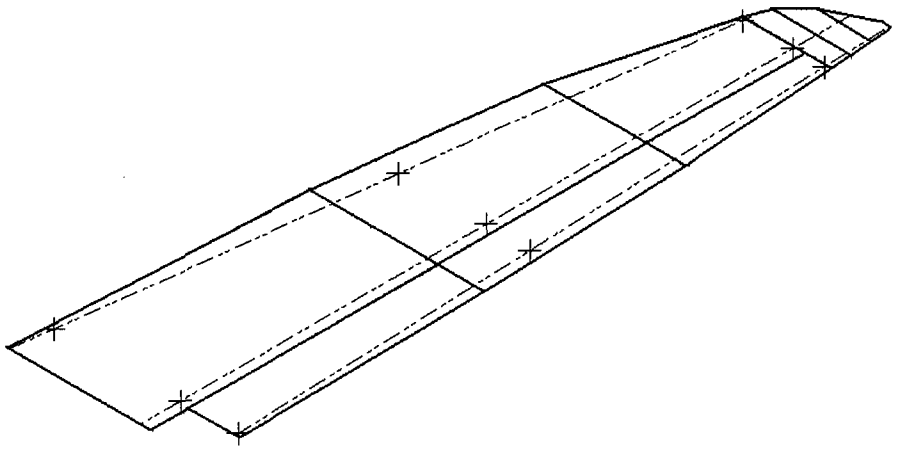

**Figure 4.3 Modal point positions on tailplane.**

Up to 20 modes can be entered in a single input file, but fewer modes are usually used. For the JS1 wing, the first three wing-bending modes and torsional modes were entered. Separate files are generated for symmetric and anti-symmetric modes. The displacements (mode shapes) for each mode is entered and are the displacements normal to the lifting surfaces. All values must be in inches for SAF only uses imperial units. Pitch rotations (rotation about the y-axis) can also be entered, in radians, although it is not necessary.

## *4.3 Results*

Results for the wings, tailplane, and fin were calculated separately for each of the two glider configurations. For the wings, results for symmetric and anti-symmetric modes were also computed separately. A structural damping of 3% was assumed in the preliminary study for the entire analysis. However, with a GVT performed in this study, the true structural damping of each mode was computed. It ranged from 0.7% to 5.6% for configuration 1 (no water) and 0.8% to 3.2% for configuration 2 (water). The analysis was performed at five altitudes: sea level, 2000 meters, 4000 meters, 6000 meters, and 8000 meters above sea level. Figure 4.4 shows the graph of the first symmetric wing bending for all five altitudes. For all the other modes analyzed, a damping vs. velocity and frequency vs. velocity graph were plotted for all five altitudes. This gives a huge amount of graphs and therefore only the graphs for sea level will be presented in this chapter.

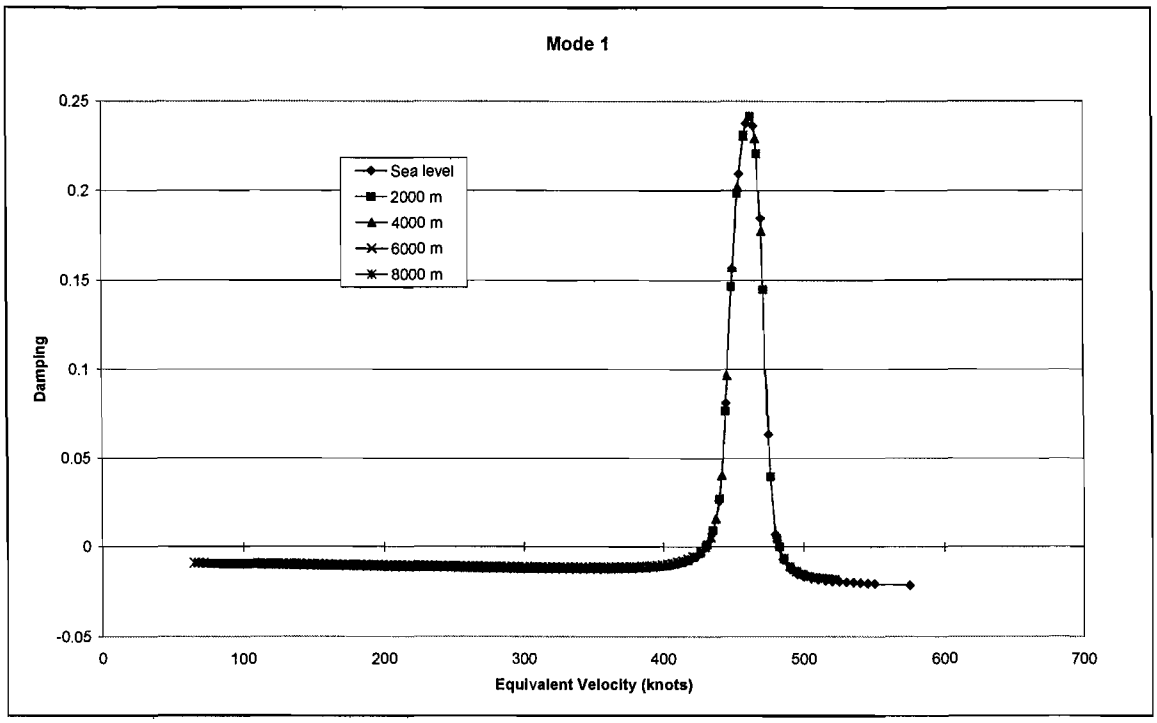


**Figure 4.4 1st Symmetric wing bending for all five altitudes.**

### 4.3.1 Configuration 1

Configuration 1 consists out of the whole glider assemblage with no water ballast in the wings. The wing modes will be presented first. Density 1, in the graphs, indicates an altitude at sea level. The symmetric wing modes' damping and frequency graphs are given in Figure 4.5 and Figure 4.6. The first wing-bending mode shows a transition from negative damping values to positive values at 430.243 knots, that is 796.810 km/h. This speed is indicated as a flutter speed. This speed is much higher than 210 knots ($1.2V_D$) and outside the glider's flight envelope.

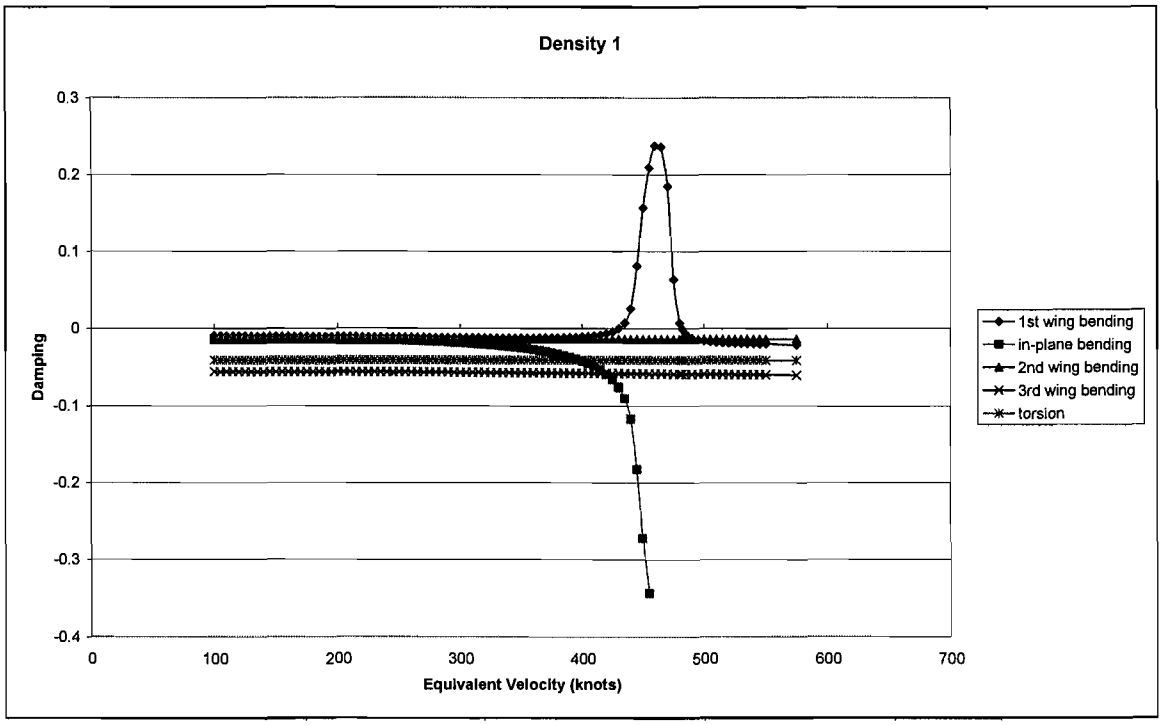


**Figure 4.5 Configuration 1, symmetric wing modes (V-g graph).**

**Table 5: Flutter speeds at all altitudes for symmetric wing modes.**

| Altitude [m] | Equivalent airspeed [knots] | True airspeed [knots] | Damping ratio |
|---|---|---|---|
| 0 | 430.243 | 430.243 | 0.000025 |
| 2000 | 430.024 | 473.814 | 0.000016 |
| 4000 | 429.762 | 525.195 | -0.000050 |
| 6000 | - | - | - |
| 8000 | - | - | - |

Table 5 gives the flutter speeds for the altitudes with the associated damping value. Figure 4.6 also shows no signs of instability up to 210 knots. The flutter speeds given in Table 5 is therefore of no concern. The in-plane bending mode shows a drop in frequency as airspeed increase. In Figure 4.5 the same mode indicates a sudden increase in negative damping. This might indicate that a divergence speed is somewhere above 400 knots. Still it is above $1.2V_D$.

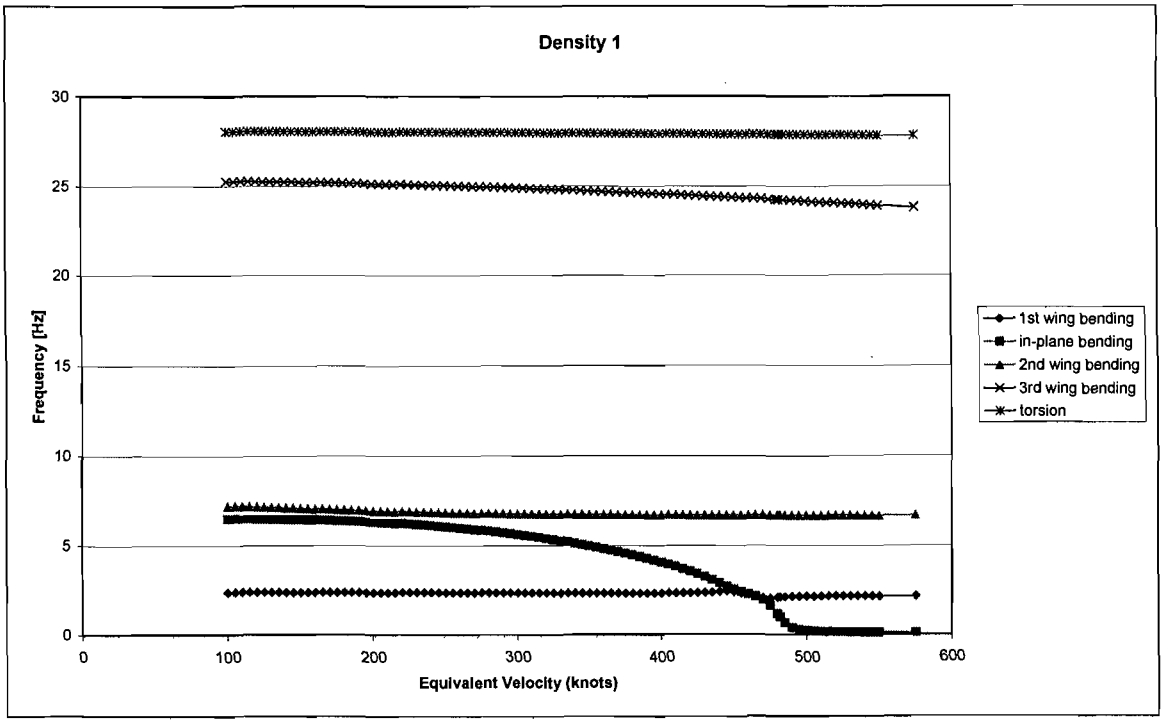


**Figure 4.6 Configuration 1, symmetric wing modes (V-Hz graph).**

The next two graphs are that of the anti-symmetric wing modes. There is no flutter speed indicated for the velocity range calculated and for all altitudes. The damping graph indicates that the first wing-bending mode has a sudden increase in negative damping. This could also possibly indicate a divergence speed. In frequency graph, the frequency is also starting to drop between 400 to 500 knots.

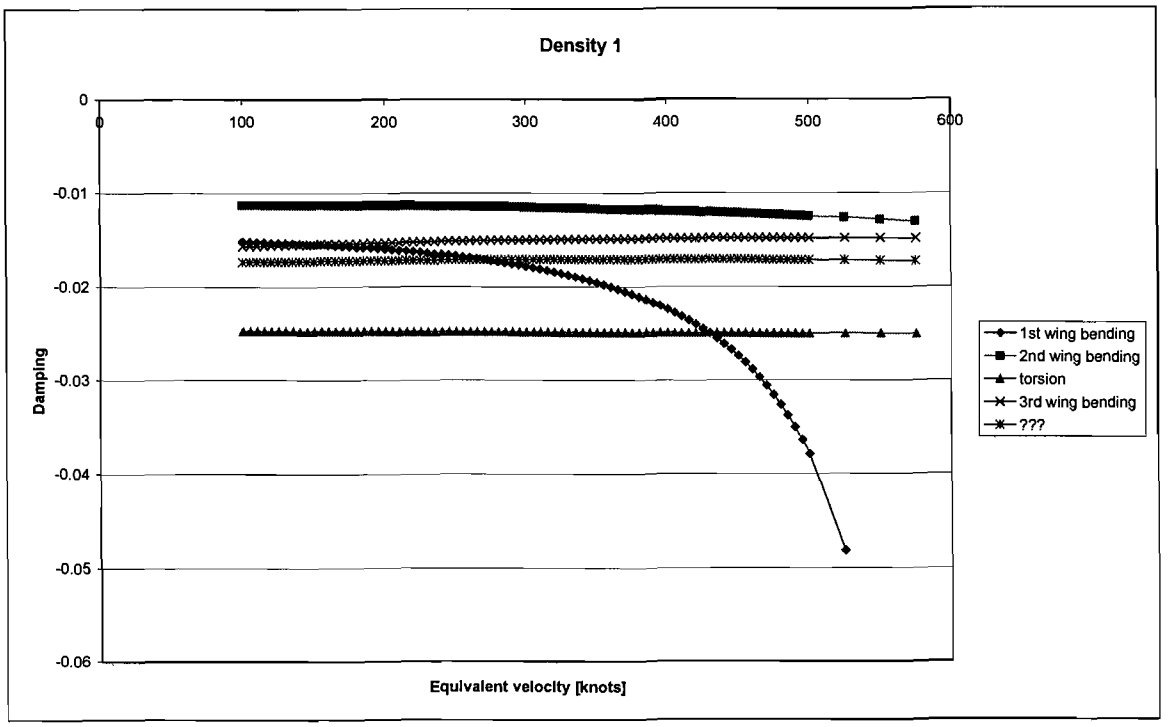


**Figure 4.7 Configuration 1, anti-symmetric wing modes (V-g graph).**

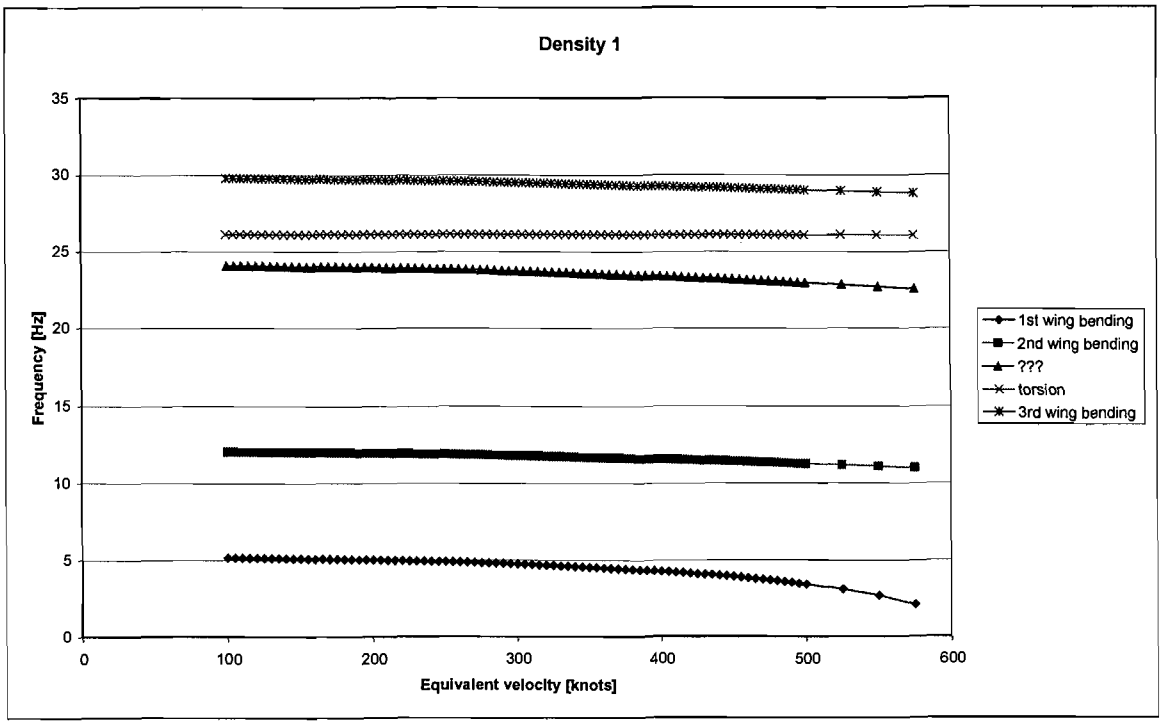


**Figure 4.8 Configuration 1, anti-symmetric wing modes (V-Hz graph).**

The next two graphs, Figure 4.9 and Figure 4.10, are the damping graph results for the fin and tailplane. For the tailplane, the one symmetric mode was included with the anti-symmetric modes in the graph, but was calculated separately from the other two.

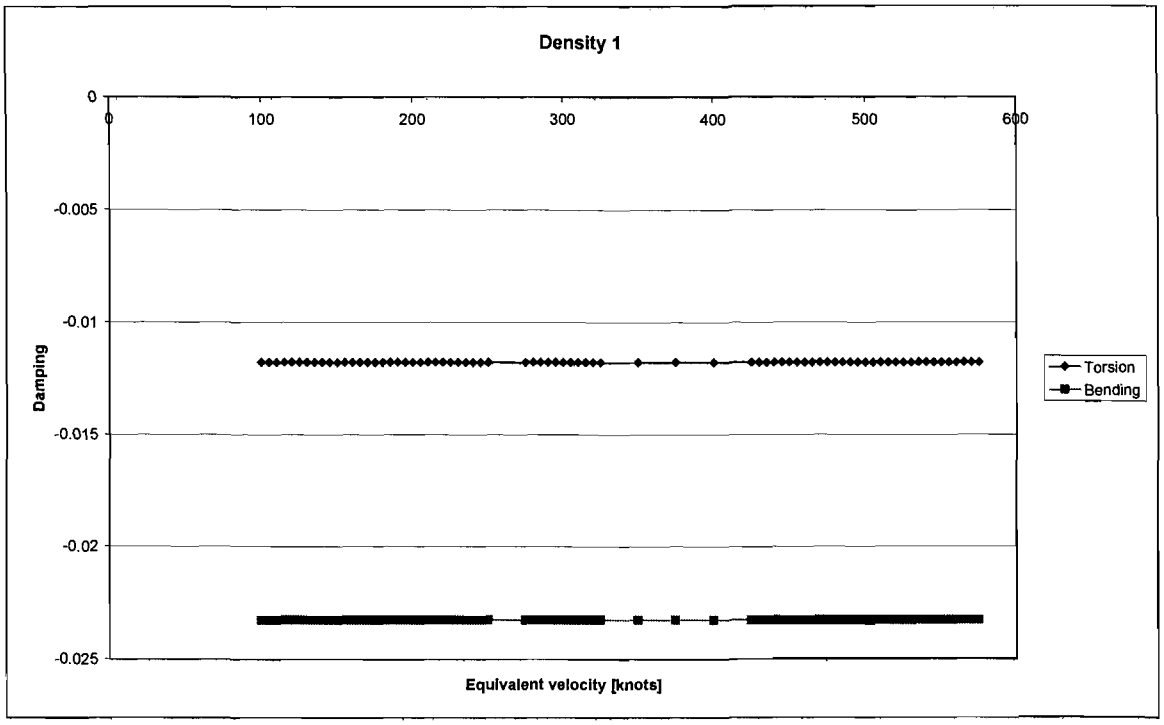


**Figure 4.9 Configuration 1, fin modes (V-g graph).**

There is also no concern of flutter for these two surfaces. The fin even shows stability up to high speeds (575 knots). Complete graphs for each glider part are given in the Appendix.

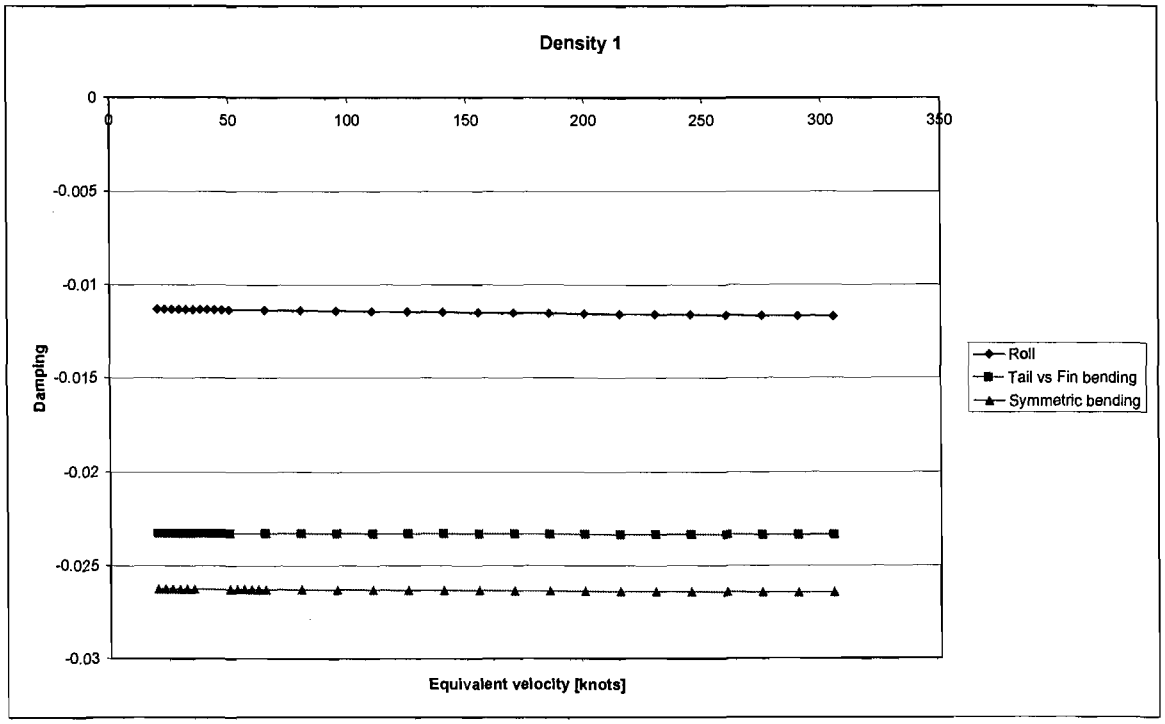


**Figure 4.10 Configuration 1, tailplane modes (V-g graph).**

### 4.3.2 Configuration 2

Configuration 2 consists out of the whole glider assemblage with water ballast in the wings. The full tanks added about 200 kg to the glider weight, equating the total weight to 600 kg. The wing modes will again be presented first.

One would expect that the peak found in Figure 4.5 made by the first wing bending, would again appear in Figure 4.11 with the flutter speed at a lower value. Instead, the first wing bending seems to get more stable because of the higher negative damping values it takes on with increase in speed. Looking at Figure 4.12 the first two modes, first wing bending and in-plane bending seems to merge around 470 knots (870.44 km/h). Still, if there were something happening at that speed it is far beyond $1.2V_D$ and therefore of no concern. This increase in negative damping values could again possibly indicate a divergence speed beyond 300 knots. Still it is of no concern for the glider.

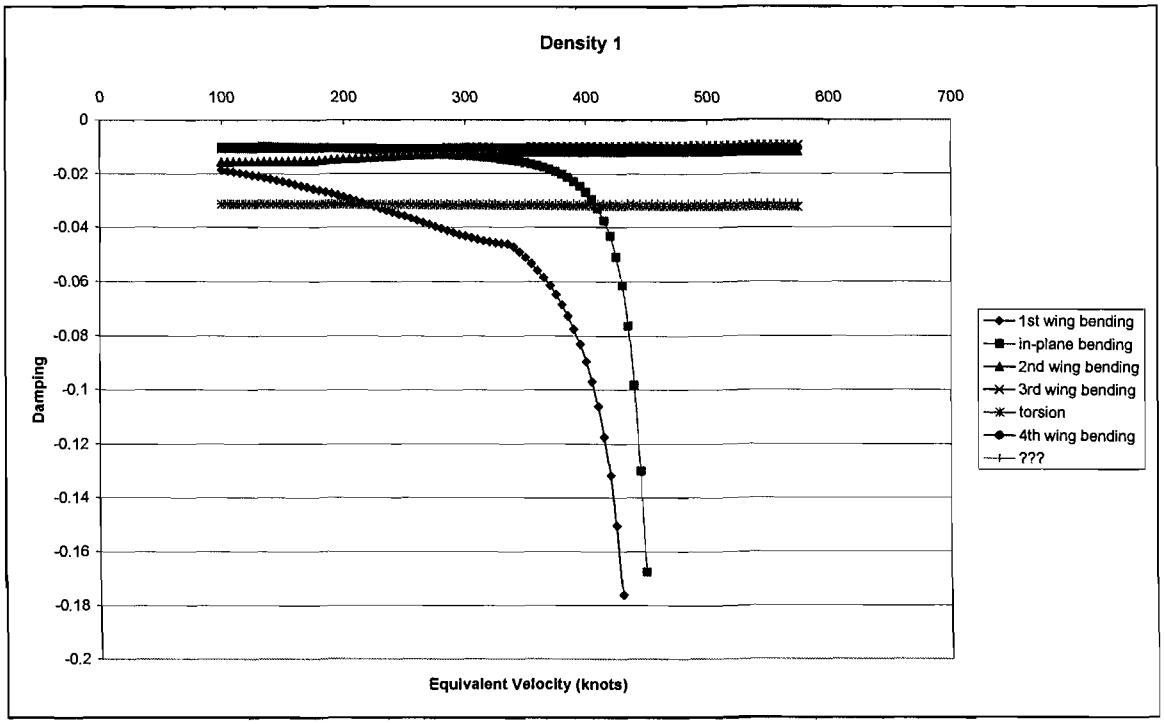


**Figure 4.11 Configuration 2, symmetric wing modes (V-g graph).**

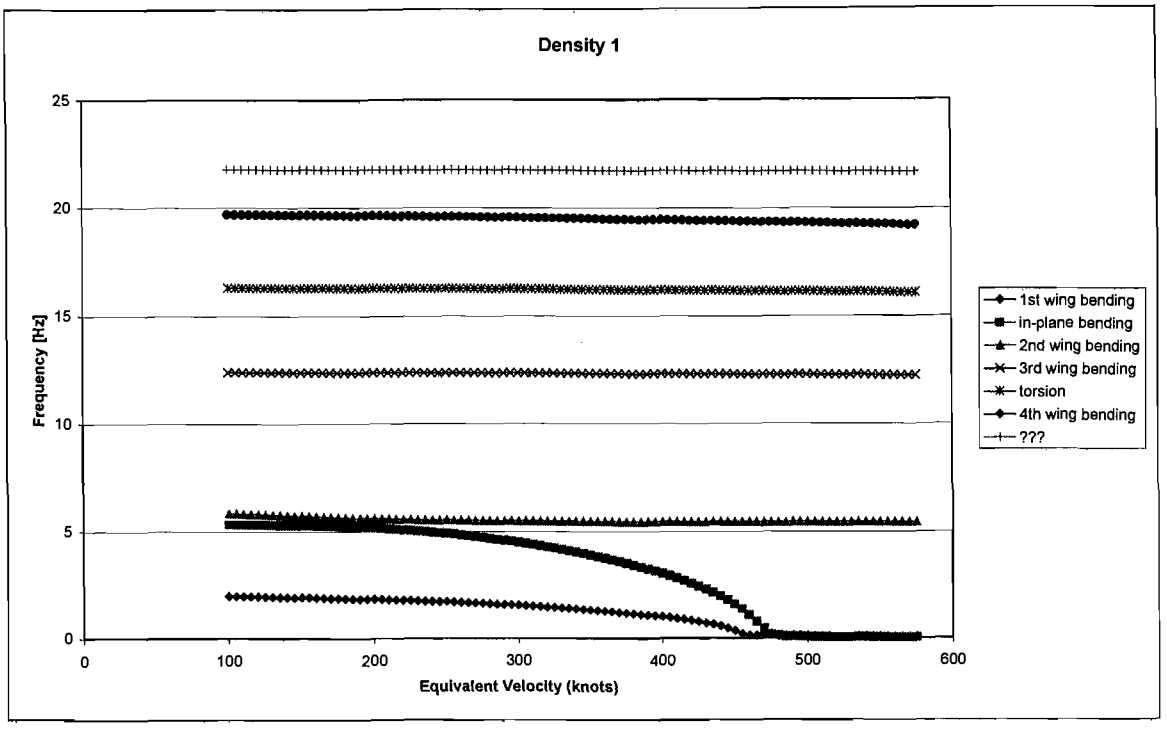


**Figure 4.12 Configuration 2, symmetric wing modes (V-Hz graph).**

Figure 4.13 and Figure 4.14 shows the anti-symmetric wing results for configuration 2. The trend looks the same as for configuration 1 (Figure 4.7).

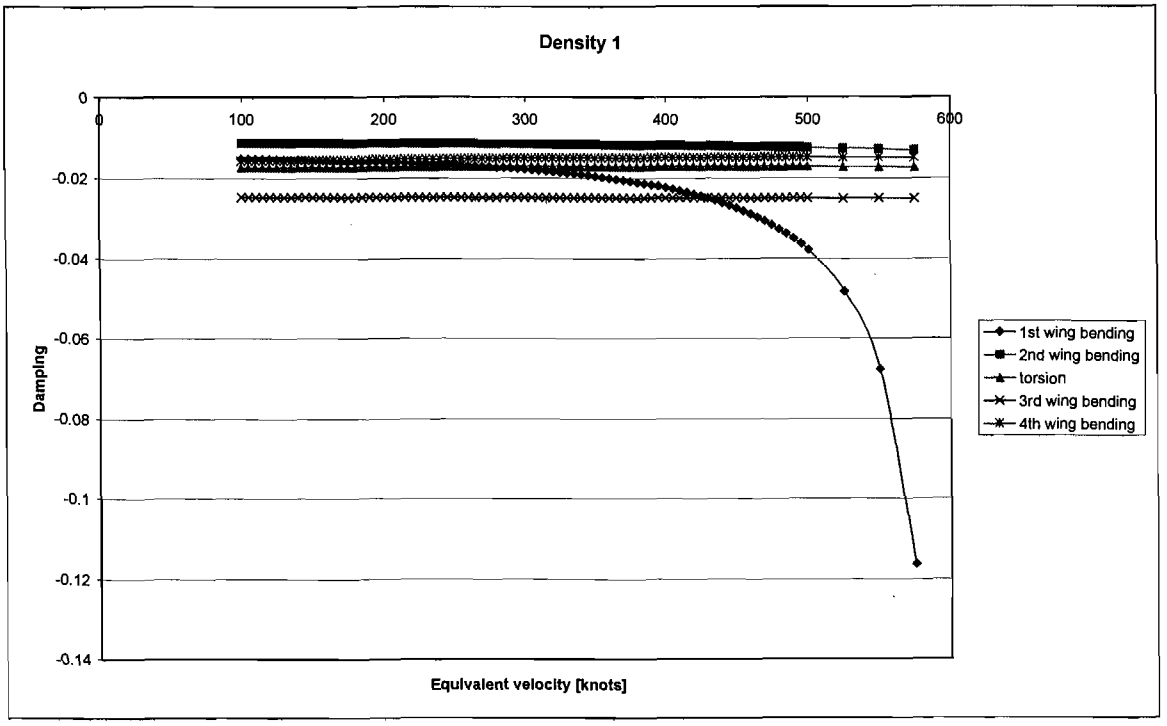


**Figure 4.13 Configuration 2, anti-symmetric wing modes (V-g graph).**

The frequency graph also shows stability over the glider's flight envelope.

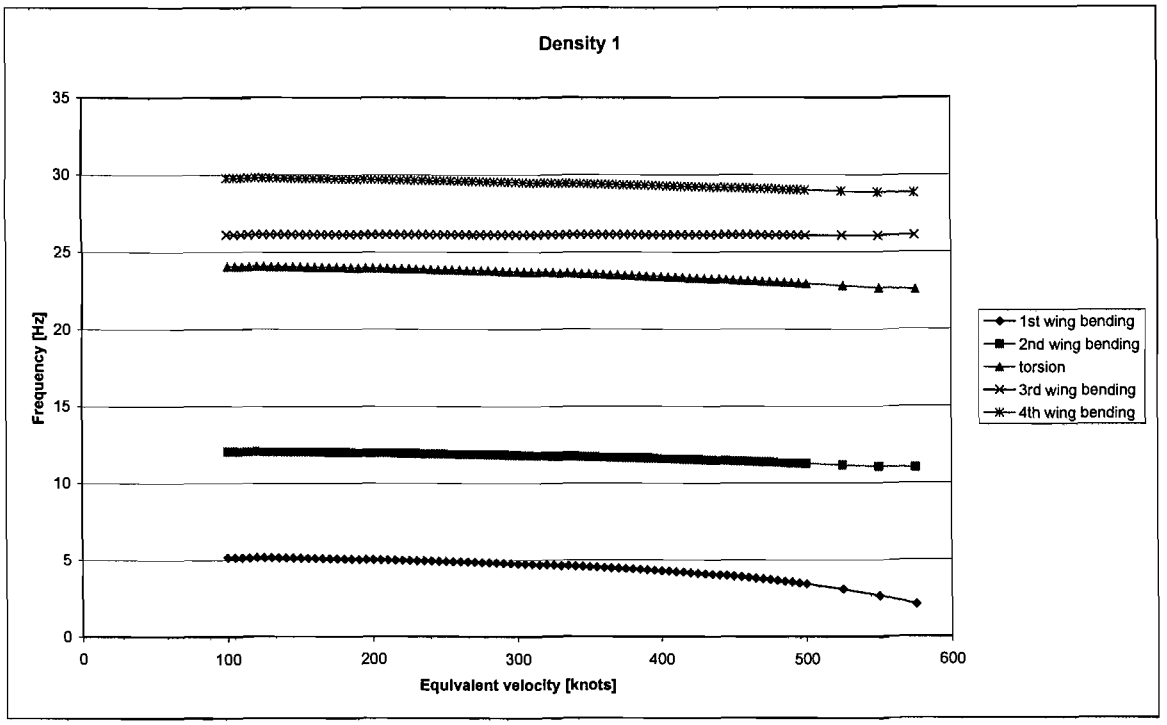


**Figure 4.14 Configuration 2, anti-symmetric wing modes (V-Hz graph).**

Fin and tailplane damping graphs is presented next. Again, the tailplane is stable over the velocity range of interest and nothing exciting is happening here.

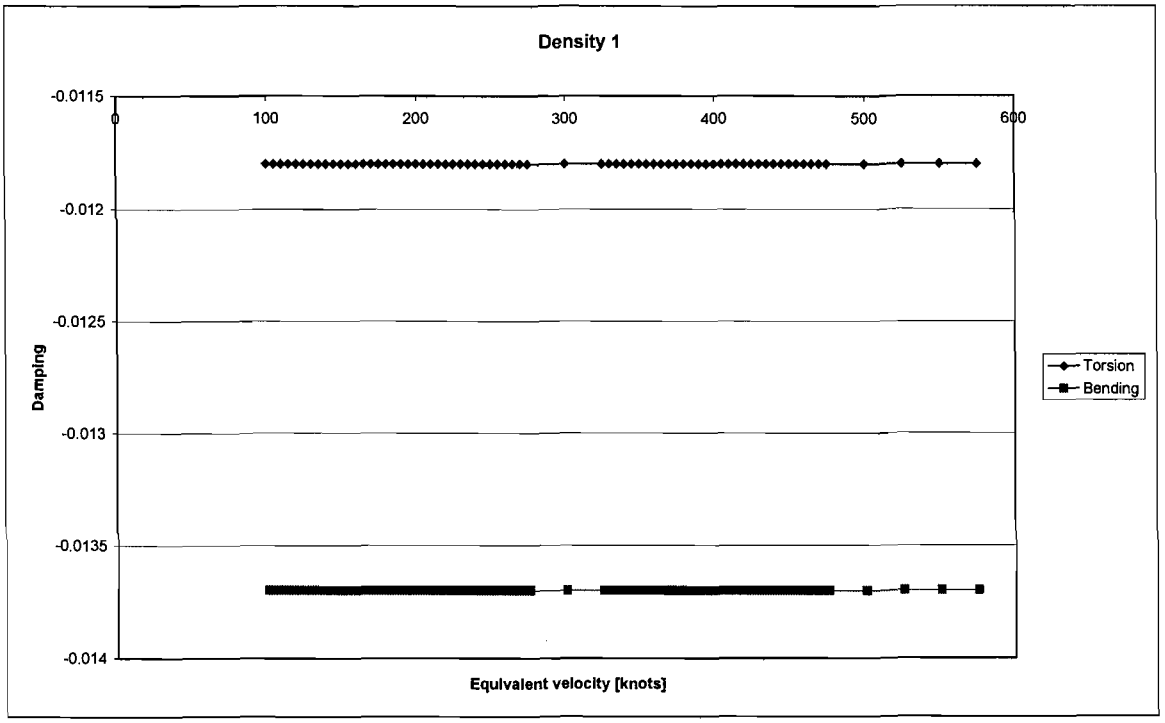


**Figure 4.15 Configuration 2, fin modes (V-g graph).**

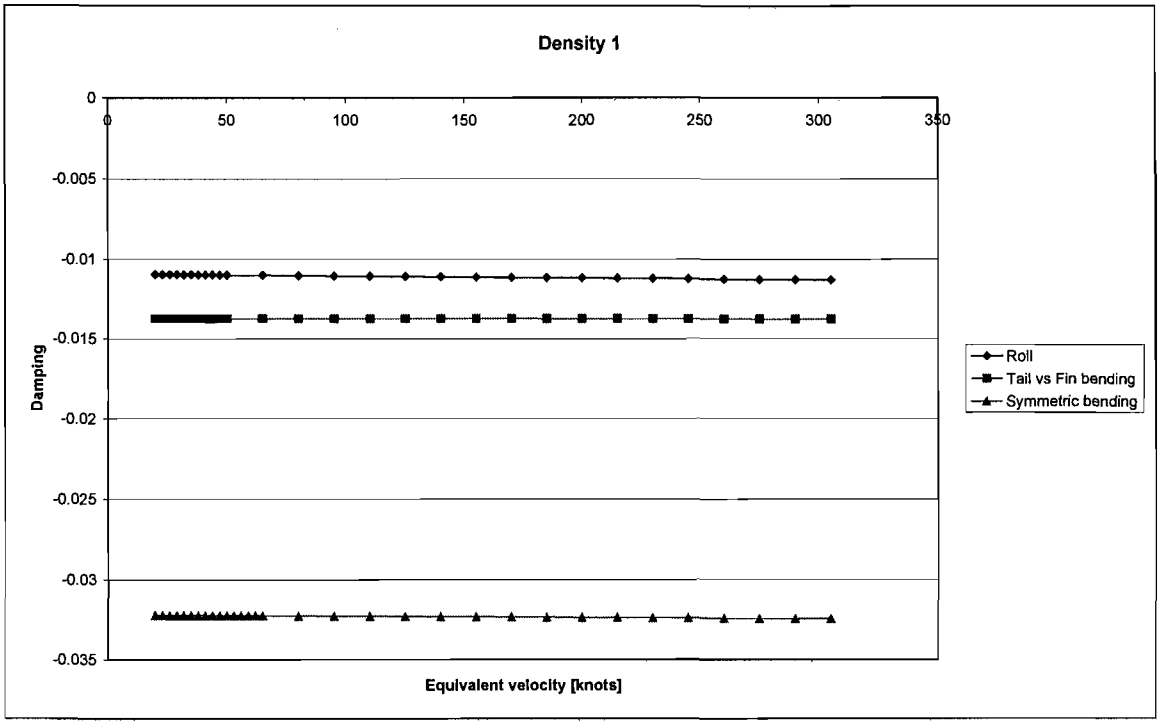


**Figure 4.16 Configuration 2, tailplane modes (V-g graph).**

All the graphs for the two glider configurations showed no flutter or instability for the desired velocity range up to 210 knots.

### 4.3.3 Comparison

In the preliminary study, there were four configurations of the glider analyzed. This included an engine. As stated earlier, no engine was installed in the JS1 prototype. So thus, only two of the four configurations can be used to compare results.

De Bruyn (2004:48) found signs of merging flutter in the region of 300 knots for the anti-symmetric results, configuration 1, where this study showed no signs of flutter. For the symmetric results, this study showed flutter around 430 knots for altitudes up to 4000 meters. The first study showed no flutter.

For configuration 2 the first study showed merging flutter for the symmetric modes at around 170 knots. Damping graphs indicated however that all modes were stable. This study showed stability over the entire glider flight envelope for these modes. For the anti-symmetric modes, both the studies showed stability and for the fin and tailplane results, both studies also showed stability for speeds up to 300 knots.

## 4.4 Summary

This chapter presented the flutter prediction analysis for the JS1 glider. The software code SAF was used to conduct the analysis. SAF makes use of a panel model of the aircraft under investigation. A panel model of the wings, tailplane, and fin of the glider was thus created. Each of these parts where analyzed separately for the reason that the text input file created for SAF could become large and difficult to handle.

SAF makes use of the doublet lattice method and the p-k algorithm was used to obtain a solution. Modes used for the flutter investigation consisted out of symmetric and anti-symmetric wing modes up to the $4^{th}$ wing-bending mode. Two modes for the fin and three for the tailplane where also investigated.

The analysis was done for altitudes from sea level with 2000-meter intervals up to 8000 meters. Unlike the preliminary study, a damping value was not assumed, for each modes' damping value where obtained from the ground vibration test. Although the first symmetric wing-bending mode for configuration 1 showed a flutter speed, this was much higher than $1.2V_D$. All the modes investigated show stability in the velocity range up to $1.2V_D$.

From this analysis, the JS1 glider is free from flutter of main surface modes in the velocity range up to 210 knots or 388.8 km/h for altitudes up 8000 meters.

# 5 CONCLUSION

A flutter analysis was conducted to find the flutter characteristics of the new prototype glider, the 18-meter class JS1 Revelation. The purpose of the analysis was to show if the glider is free from flutter within its design envelope and forms part of the certification process of the glider. The main lifting surfaces of the glider were investigated. The information gained through the analysis could be used in later flutter flight tests. The whole analysis was performed in two parts. First, a modal analysis was done followed by a flutter prediction.

A modal analysis was performed by means of a ground vibration test. The complete glider was tested with two configurations: with no water ballast and with water ballast in the wings. This practical determination of the dynamic characteristics of the glider was done because a preliminary study was done earlier by using finite element modelling.

For each of the two configurations the 1$^{st}$, 2$^{nd}$ and 3$^{rd}$ symmetric and anti-symmetric wing bending modes and wing torsion modes were extracted as well as fin, stabilizer, and fuselage modes. The 4$^{th}$ symmetric and anti-symmetric wing bending modes for configuration 2 were also extracted during the test. Two unknown torsional modes were also found. All of these modes were extracted in the frequency range 1 Hz – 32 Hz. The natural frequency, modal damping, and mode shape of each mode are among the modal results.

Modal results from this study did not compare well with the results from the preliminary study. The reason could be that structural changes were made to the glider during the time between the two studies.

The flutter prediction was done with the software code SAF (Subsonic Aerodynamic Flutter). The modal results found in the GVT were used in the input file for SAF. SAF made use of a panel model of the glider and utilized the doublet lattice method and p-k solution method. The wings were analyzed separately from the fin and tailplane. The analysis was done for altitudes from sea level up to 8000 meters.

The flutter results from the flutter code were a series of frequency and damping versus airspeed graphs. There was one case of flutter around a speed of 430 knots for the symmetric wing bending modes, configuration 1. Results however indicated stability of main surface modes in the velocity range up to $1.2V_D$ (210 knots) up to an altitude of 8000 meters.

## 5.1 Recommendations

The modes found during the ground vibration test included only main surface modes. That is modes of the wing surface, tailplane surface and fin surface. It did not include any control surface modes because no such modes where found in the frequency range investigated. It could be that these modes occur at higher frequencies or that another method should be used to investigate it. However, although no control surface modes where found, basic control surface modes could have been included in the analysis. The mode shape is simply the control surface rotation. The modal mass could be estimated from component masses.

Control surfaces are used to control an aircraft and it is therefore important to determine if it may present a vibration problem within the aircraft's velocity range. The characteristics of the behaviour of the control surface must thus be determined.

# 6 APPENDIX

## 6.1 Positions of modal points on glider

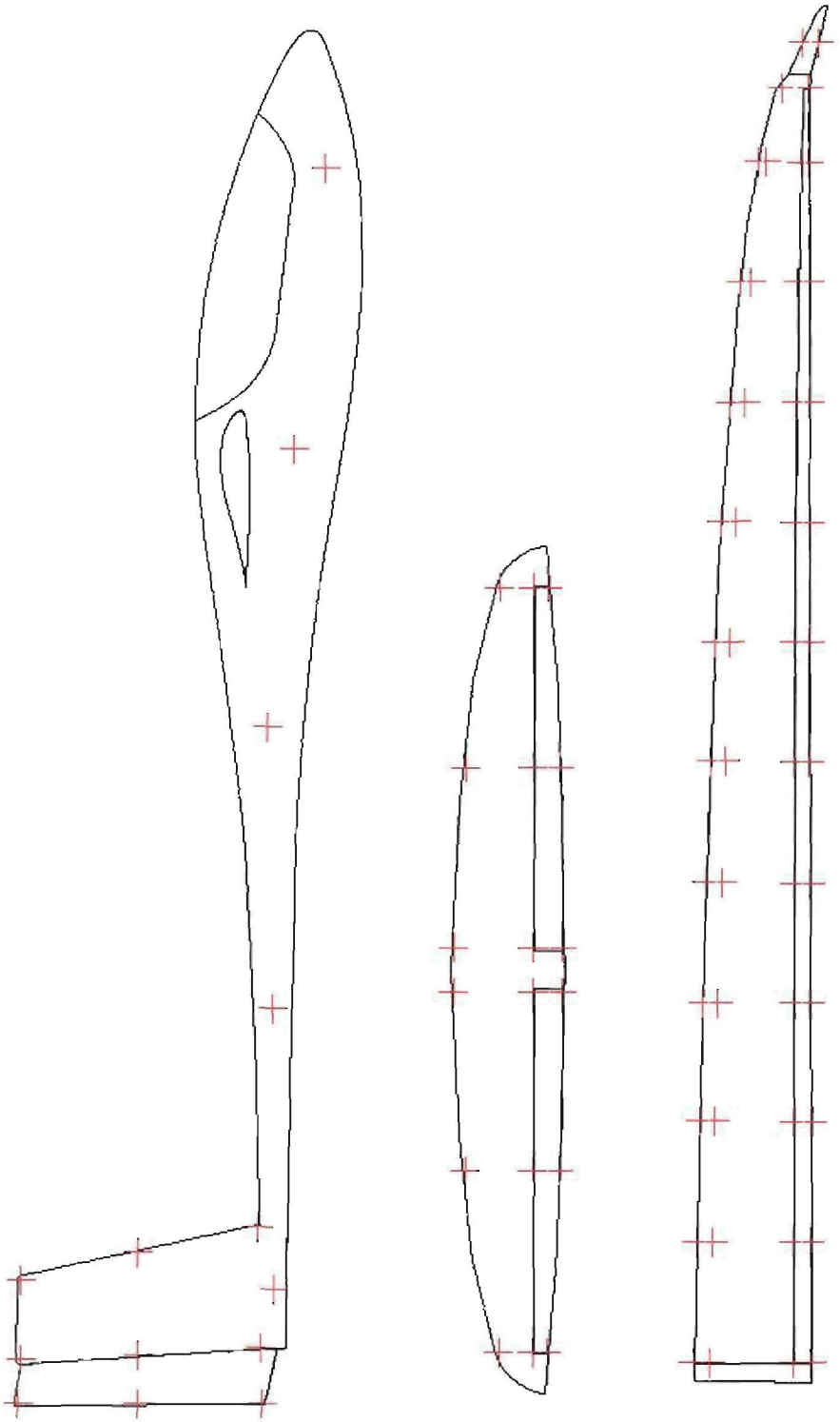

## 6.2 *Modal parameters from the GVT*

| Mode description | 2nd GVT (no water) | | | 2nd GVT (water) | | |
|---|---|---|---|---|---|---|
| | Frequency [Hz] | Damping [-] | Modal mass [kg] | Frequency [Hz] | Damping [-] | Modal mass [kg] |
| 1st Symmetric wing bending | 2.403 | 0.00841 | 140.761 | 2.045 | 0.01492 | 1177.769 |
| 2nd Symmetric wing bending | 7.336 | 0.01405 | 214.021 | 5.952 | 0.01586 | 552.434 |
| 3rd Symmetric wing bending | 25.327 | 0.05621 | 105.965 | 12.397 | 0.01068 | 2440.892 |
| 4th Symmetric wing bending | - | - | - | 19.715 | 0.01063 | 380.871 |
| Symmetric wing torsion | 28.056 | 0.04120 | 191.568 | 16.298 | 0.03134 | 260.498 |
| Symmetric wing in-plane bending | 6.547 | 0.01294 | 463.118 | 5.358 | 0.01004 | 1111.657 |
| Symmetric *unknown* | - | - | - | 21.770 | 0.03117 | 165.424 |
| | | | | | | |
| 1st Anti-symmetric wing bending | 5.201 | 0.01496 | 687.022 | 3.970 | 0.01271 | 1134.051 |
| 2nd Anti-symmetric wing bending | 12.082 | 0.01128 | 131.470 | 9.409 | 0.01044 | 983.617 |
| 3rd Anti-symmetric wing bending | 29.838 | 0.01588 | 220.533 | 16.668 | 0.01210 | 653.878 |
| 4th Anti-symmetric wing bending | - | - | - | 26.354 | 0.01118 | 947.487 |
| Anti-symmetric wing torsion | 26.125 | 0.02469 | 123.504 | 19.087 | 0.01809 | 199.228 |
| Anti-symmetric *unknown* | 24.117 | 0.01750 | 156.037 | - | - | - |
| | | | | | | |
| Fuselage vertical bending | 11.821 | 0.00730 | 240.350 | 10.955 | 0.01034 | 613.112 |
| Fuselage horizontal bending | 19.179 | 0.02013 | 74.567 | 17.586 | 0.01504 | 160.551 |
| Fuselage torsion | 4.470 | 0.00925 | 73.222 | 4.549 | 0.00804 | 109.266 |
| | | | | | | |
| Fin torsion | 12.601 | 0.01178 | 42.325 | 11.998 | 0.01180 | 49.399 |
| | | | | | | |
| Stabilizer roll | 8.703 | 0.01129 | 9.636 | 8.226 | 0.01095 | 10.916 |
| Stabilizer vs. fin bending | 14.539 | 0.02328 | 25.223 | 13.410 | 0.01370 | 62.820 |
| Stabilizer symmetric bending | 21.162 | 0.02625 | 3.463 | 21.139 | 0.03223 | 3.678 |

## 6.3 Wing input file for SAF

For paragraph 6.3, 6.4 and 6.5 the following is applicable:

## - Indicate where the mode frequencies are entered.

### - Indicate where mode displacements are entered.

#### - Indicate where modal damping of each mode is entered.

```
1
FLUTTER ANALYSIS OF THE JS1 WING
15 PANELS, 1 CONTROL SURFACE, 315 ELEMENTS TOTAL
SYMMETRIC CASE
P-K METHOD
5 VIBRATION MODES
MACH = 0.264 (Vd)
**[1] [2] [3] [4] [5] [6] [7] [8] [9] [10]
-1  5  2  6  5  0  0  0  0  0
 1  0  1  0  0 -1  0  0  1  0
 1  0  0  1  0  0  0  0  0  0
 0  0  0  0  0  0  0
 37
 ###
 2
 1  1  ##  2  2  ##  3  3  ##
 4  4  ##  5  5  ##
 2.403  6.547  7.336  25.327  28.056
 15.485  0.264
 20  100  25
 0.02  0.5  1  5  10  15  50
 5
 1  ####
 2  ####
 3  ####
 4  ####
 5  ####
 0.5 -2  600  50
 1  0.8237  0.6696  0.5361  0.4216
 30.9699  1
 1  15  0  1260  0  0  1
**PANEL 1
 0  0  0  0
 77.0418  108.0709  77.1041  108.0117  12.5984  17.4118
 5.6965  5.8461  3  8  0
 0  0.2107  0.4214  0.6322  0.8429  0.8953
 0.9476  1
 0  0.5  1
**PANEL 2
 0  0  0  0
 77.1041  103.1555  78.458  102.2532  17.4118  121.9696
 5.8461  9.0948  11  5  0
 0  0.125  0.5  0.75  1
 0  0.1  0.2  0.3  0.4  0.5
 0.6  0.7  0.8  0.9  1
**PANEL 3
 0  0  0  0
 78.458  102.2532  81.0473  101.4496  121.9696  224.3307
 9.0948  12.7056  11  5  0
 0  0.125  0.5  0.75  1
 0  0.1  0.2  0.3  0.4  0.5
 0.6  0.7  0.8  0.9  1
**PANEL 4
 0  0  0  0
 81.0473  101.4496  85.7366  101.6862  224.3307  295.1968
 12.7056  17.9591  8  5  0
 0  0.125  0.5  0.75  1
 0  0.1429  0.2857  0.4286  0.5714  0.7143
```

```
0.8571  1
**PANEL 5
 0  0  0  0
 85.7366  101.6862  88.1688  101.9055  295.1968  316.7592
 17.9591  21.1712  4  5  0
 0  0.125  0.5  0.75  1
 0  0.333  0.6667  1
**PANEL 6
 0  0  0  0
 88.1688  101.9055  91.4662  102.1345  316.7592  336.4996
 21.1712  24.0833  4  5  0
 0  0.125  0.5  0.75  1
 0  0.333  0.6667  1
**PANEL 7
 0  0  0  0
 91.4662  102.1345  94.8835  102.5079  336.4996  349.7657
 24.0833  29.9898  4  5  0
 0  0.125  0.5  0.75  1
 0  0.333  0.6667  1
**PANEL 8
 0  0  0  0
 94.8835  103.9229  98.3374  104.2386  349.7657  352.7819
 29.9898  32.7276  3  8  0
 0  0.1429  0.2857  0.4286  0.5714  0.7143
 0.8571  1
 0  0.5  1
**PANEL 9
 0  0  0  0
 98.3374  104.2386  105.6441  108.0787  352.7819  354.2191
 32.7276  49.1563  6  8  0
 0  0.1429  0.2857  0.4286  0.5714  0.7143
 0.8571  1
 0  0.2  0.4  0.6  0.8  1
**PANEL 10
 0  0  0  0
 103.1555  108.0117  102.2532  106.7272  17.4118  121.9696
 5.8461  9.0948  11  4  0
 0  0.333  0.6667  1
 0  0.1  0.2  0.3  0.4  0.5
 0.6  0.7  0.8  0.9  1
**PANEL 11
 0  0  0  0
 102.2532  106.7272  101.4496  105.2574  121.9696  224.3307
 9.0948  12.7056  11  4  0
 0  0.333  0.6667  1
 0  0.1  0.2  0.3  0.4  0.5
 0.6  0.7  0.8  0.9  1
**PANEL 12
 0  0  0  0
 101.4496  105.2574  101.6862  104.595  224.3307  295.1968
 12.7056  17.9591  8  4  0
 0  0.333  0.6667  1
 0  0.1429  0.2857  0.4286  0.5714  0.7143
 0.8571  1
**PANEL 13
 0  0  0  0
 101.6862  104.595  101.9055  104.409  295.1968  316.7592
 17.9591  21.1712  4  4  0
 0  0.333  0.6667  1
 0  0.333  0.6667  1
**PANEL 14
 0  0  0  0
 101.9055  104.409  102.1345  104.0646  316.7592  336.4996
 21.1712  24.0833  4  4  0
 0  0.333  0.6667  1
 0  0.333  0.6667  1
**PANEL 15
 0  0  0  0
 102.1345  104.0646  102.5079  103.9229  336.4996  349.7657
 24.0833  29.9898  4  4  0
 0  0.333  0.6667  1
 0  0.333  0.6667  1
***END OF REPEAT
 1  0  0  0  0  0
 1  315  0
```

```
F 207  0
 10  0  1  1
**LINE 1
 4  80.8139  0.0001  82.267  355
 17.7733  49.2574  80.7414  112.2255
**LINE 2
 3  82.9419  143.7065  84.5345  206.6659
 143.7065  175.1862  84.5345
**LINE 3
 2  85.8942  238.1164  87.9729  269.5295
 238.1164  269.5295
**LINE 4
 2  89.134  300.8956  92.6916  332.0544
 300.8956  332.0544
**LINE 5
 2  96.599  350.0414  102.0638  353.4866
 350.0414  353.4866
**LINE 6
 4  103.1104  0.0001  102.1418  355
 17.7733  49.2574  80.7414  112.2255
**LINE 7
 3  101.887  143.7065  101.3927  206.6659
 143.7065  175.1862  84.5345
**LINE 8
 2  101.2983  238.1164  101.4031  269.5295
 238.1164  269.5295
**LINE 9
 2  101.5457  300.8956  101.8842  332.0544
 300.8956  332.0544
**LINE 10
 2  103.7407  350.0414  106.1586  353.5173
 350.0414  353.4866
F 108  0
 4  0  1  1
**LINE 11
 4  108.0308  0.0001  106.6521  355
 17.7733  49.2574  80.7414  112.2255
**LINE 12
 3  106.2206  143.7065  105.3166  206.6659
 143.7065  175.1862  84.5345
**LINE 13
 2  104.9332  238.1164  104.6396  269.5295
 238.1164  269.5295
**LINE 14
 2  104.3504  300.8956  103.9481  332.0544
 300.8956  332.0544
  ***END OF REPEAT - LINES
 1
```

## 6.4 Tailplane input file for SAF

```
1
FLUTTER ANALYSIS OF THE JS1 TAILPLANE
9 PANELS, 1 CONTROL SURFACE, 185 ELEMENTS TOTAL
ANTI-SYMMETRIC CASE
P-K METHOD
3 VIBRATION MODES
MACH = 0.264  (Vd)
**[1] [2] [3] [4] [5] [6] [7] [8] [9] [10]
-1  3  2  6  5  0  0  0  0  0
 1  0  1  0  0 -1  0  0  1  0
 1  0  0  1  0  0  0  0  0  0
 0  0  0  0  0  0  0
 9
 ###
 1
 1  1  ##  2  2  ##  3  3  ##
 8.703  14.539  21.162
 8.196  0.264
 20  20  15
 0.02  0.5  1  5  10  15  50
 3
 1  ####
 2  ####
 3  ####
 0.5  -2  600  100
 1  0.8237  0.6696  0.5361  0.4216
 16.391  1
-1  9  0  185  0  0  1
**PANEL 1
 0  0  0  0
 0  11.9977  1.2744  11.9977  0  24.1943
 0  0  8  6  0
 0  0.2  0.4  0.6  0.8  1
 0  0.14144  0.28289  0.42433  0.56578  0.70722
 0.85361  1
**PANEL 2
 0  0  0  0
 1.2744  11.9977  3.3232  11.9977  24.1943  41.871
 0  0  6  6  0
 0  0.2  0.4  0.6  0.8  1
 0  0.2  0.4  0.6  0.8  1
**PANEL 3
 0  0  0  0
 3.3232  11.9977  6.6483  11.9977  41.871  55.1181
 0  0  6  6  0
 0  0.2  0.4  0.6  0.8  1
 0  0.2  0.4  0.6  0.8  1
**PANEL 4
 0  0  0  0
 6.6483  14.2122  7.4618  14.0654  55.1181  56.9921
 0  0  3  8  0
 0  0.12774  0.27312  0.41849  0.56387  0.70925
 0.85462  1
 0  0.5  1
**PANEL 5
 0  0  0  0
 7.4618  14.0654  9.1728  13.9186  56.9921  58.8661
 0  0  3  8  0
 0  0.12774  0.27312  0.41849  0.56387  0.70925
 0.85462  1
 0  0.5  1
**PANEL 6
 0  0  0  0
 9.1728  13.9186  12.9848  13.7718  58.8661  60.7402
 0  0  3  5  0
 0  0.25  0.5  0.75  1
 0  0.5  1
**PANEL 7
 0  0  0  0
```

```
11.9977  16.391  11.9977  16.0202  3.0906  24.1943
0  0  7  5  0
0  0.25  0.5  0.75  1
0  0.16667  0.33333  0.5  0.66667  0.83333
1
**PANEL 8
0  0  0  0
11.9977  16.0202  11.9977  15.3309  24.1943  41.871
0  0  6  5  0
0  0.25  0.5  0.75  1
0  0.2  0.4  0.6  0.8  1
**PANEL 9
0  0  0  0
11.9977  15.3309  11.9977  14.2122  41.871  55.1181
0  0  6  5  0
0  0.25  0.5  0.75  1
0  0.2  0.4  0.6  0.8  1
***END OF REPEAT
1  0  0  0  0  1
1  185  0
F  121  0
2  0  1  1
**LINE 1
3  0.1575  0  7.8873  62
3.2874  29.1043  54.9213
**LINE 2
3  11.2103  0  11.2103  62
3.2874  29.1043  54.9213
F  64  0
1  0  1  1
**LINE 4
3  16.1313  0  13.5376  62
3.2874  29.1043  54.9213
  ***END OF REPEAT - LINES
1
```

## 6.5 Fin input file for SAF

```
1
FLUTTER ANALYSIS OF THE JS1 FIN
2 PANELS, 1 CONTROL SURFACE, 64 ELEMENTS TOTAL
NO SYMMETRY
P-K METHOD
1 VIBRATION MODE
MACH = 0.264  (Vd)
**[1] [2] [3] [4] [5] [6] [7] [8] [9] [10]
-1  2  2  6  5  0  0  0  0  0
 1  0  1  0  0 -1  0  0  1  0
 1  0  0  1  0  0  0  0  0  0
 0  0  0  0  0  0  0
 9
 ###
 1
 1  1  ##  2  2  ##
 12.601   14.539
 18.222   0.264
 20   100   25
 0.02   0.5   1   5   10   15   50
 2
 1  ####
 2  ####
 0.5  -2   600   50
 1  0.8237   0.6696   0.5361   0.4216
 36.4441   1
 0  2  0  128  0  0  1
**PANEL 1
 0  0  0  90
 2.1863   27.3789   12.2353   29.898   2.3103   51.8895
 0  0  9  6  0
 0  0.2   0.4   0.6   0.8   1
 0  0.125   0.25   0.375   0.5   0.625
 0.75   0.875   1
**PANEL 2
 0  0  0  90
 27.3789   38.6304   29.898   38.1559   2.3103   51.8895
 0  0  9  4  0
 0  0.333   0.6667   1
 0  0.125   0.25   0.375   0.5   0.625
 0.75   0.875   1
**END OF REPEAT
 1  0  0  0  0  0
 1  64  0
F  40  0
 2  0  1  1
**LINE 1
 3  3.3947   0   12.6244   51.8895
 2.8154   27.0999   12.5345
**LINE 2
 3  26.0789   0   28.7154   51.8895
 2.8154   27.0999   12.5345
F  24  0
 1  0  1  1
**LINE 3
 3  38.2588   0   37.7622   51.8895
 2.8154   27.0999   12.5345
   ***END OF REPEAT - LINES
 1
```

## 6.6 *Flutter graphs*

| Configuration | Glider components | | | | Weight [kg] |
|---|---|---|---|---|---|
| 1 | Fuselage | Wings | Tailplane | | 400 |
| 2 | Fuselage | Wings | Tailplane | Water ballast | 600 |

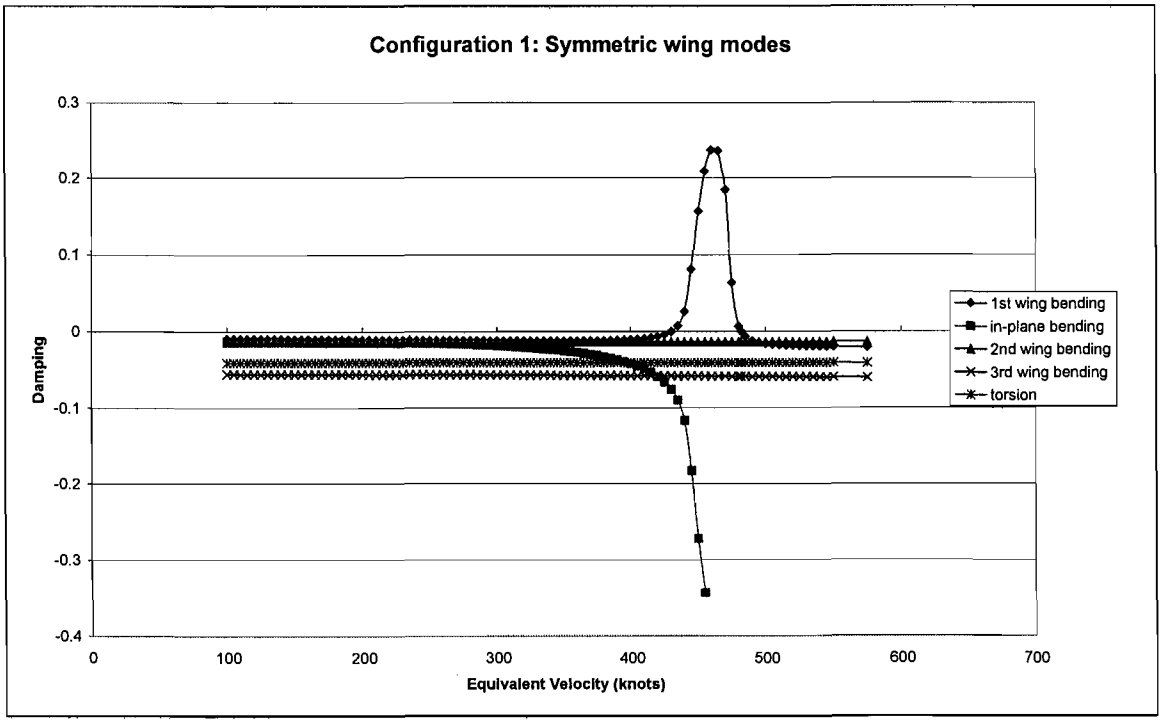


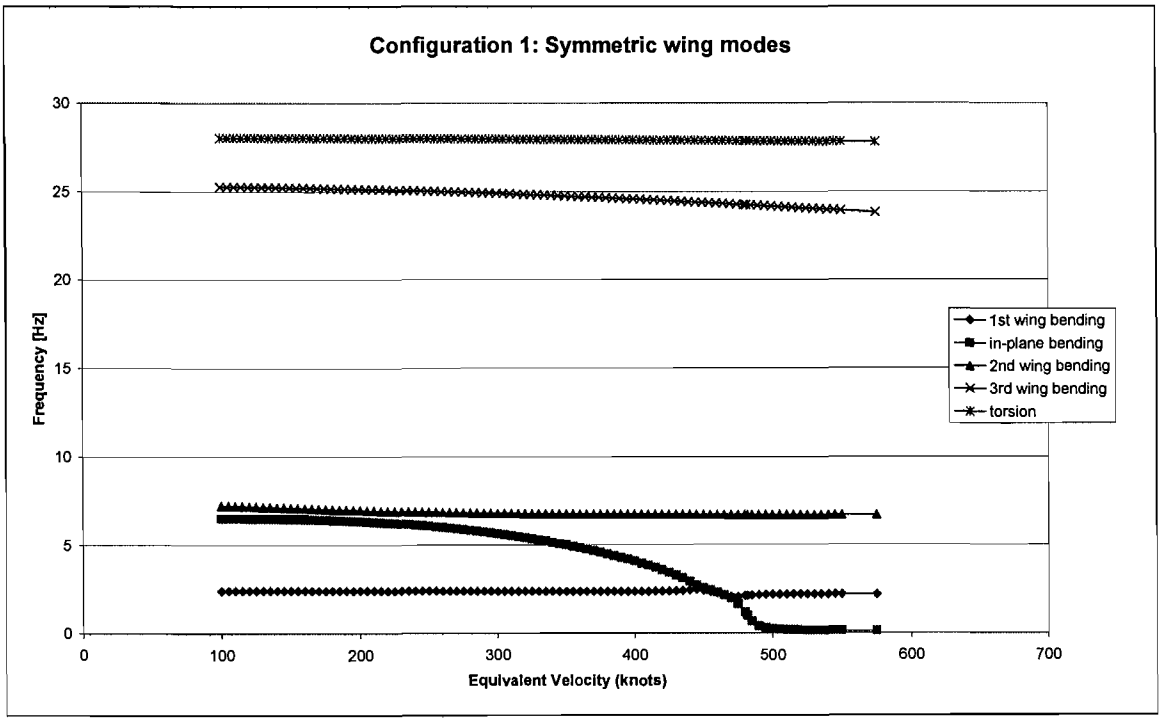

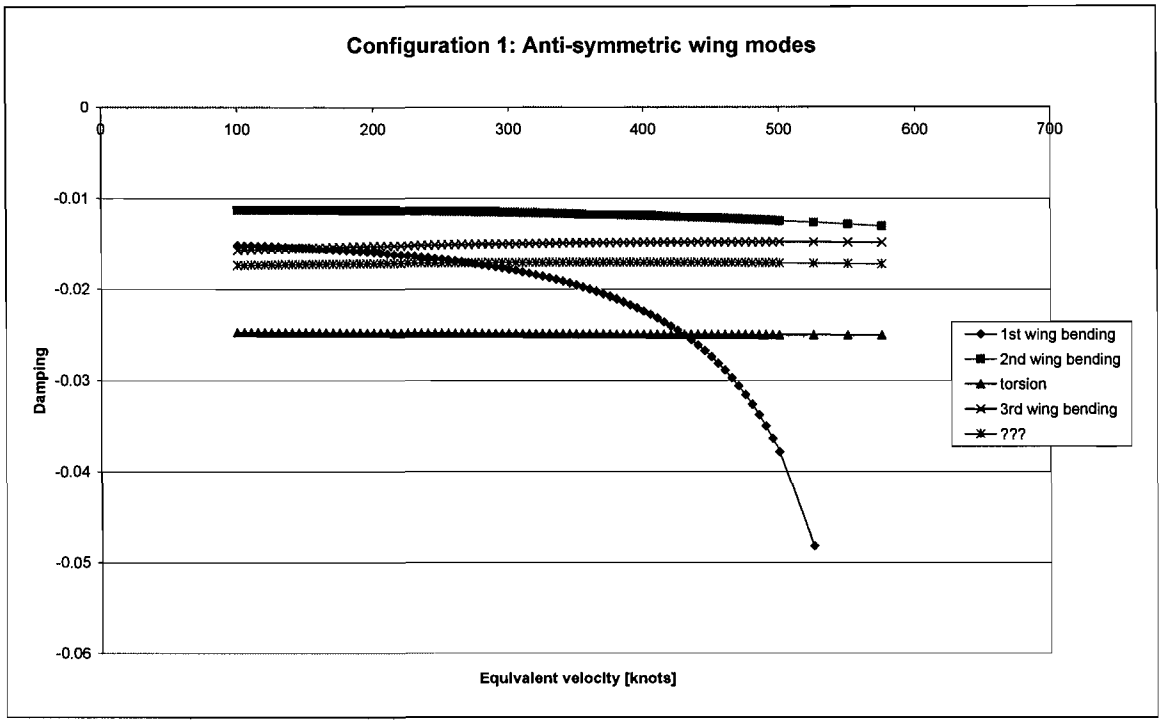
Configuration 1: Anti-symmetric wing modes
0
-0.01
-0.02
-0.03
-0.04
-0.05
-0.06
Damping
0
100
200
300
400
500
600
700
Equivalent velocity [knots]
1st wing bending
2nd wing bending
torsion
3rd wing bending
???

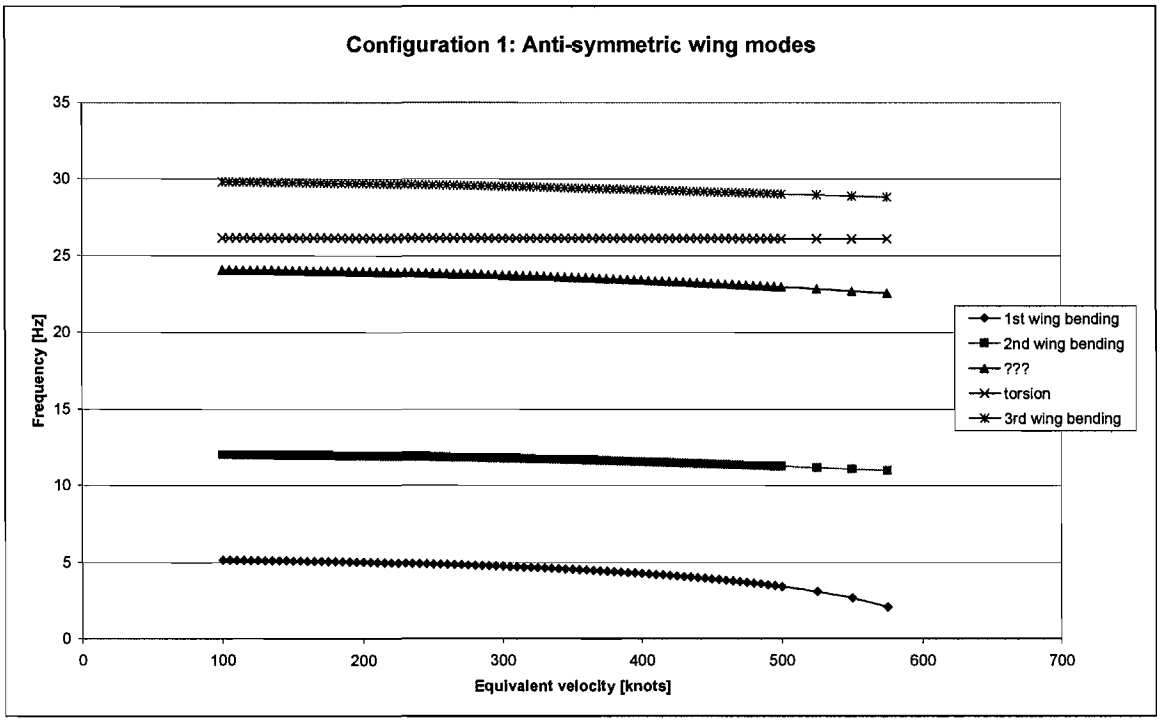
Configuration 1: Anti-symmetric wing modes
35
30
25
20
15
10
5
0
Frequency [Hz]
0
100
200
300
400
500
600
700
Equivalent velocity [knots]
1st wing bending
2nd wing bending
???
torsion
3rd wing bending

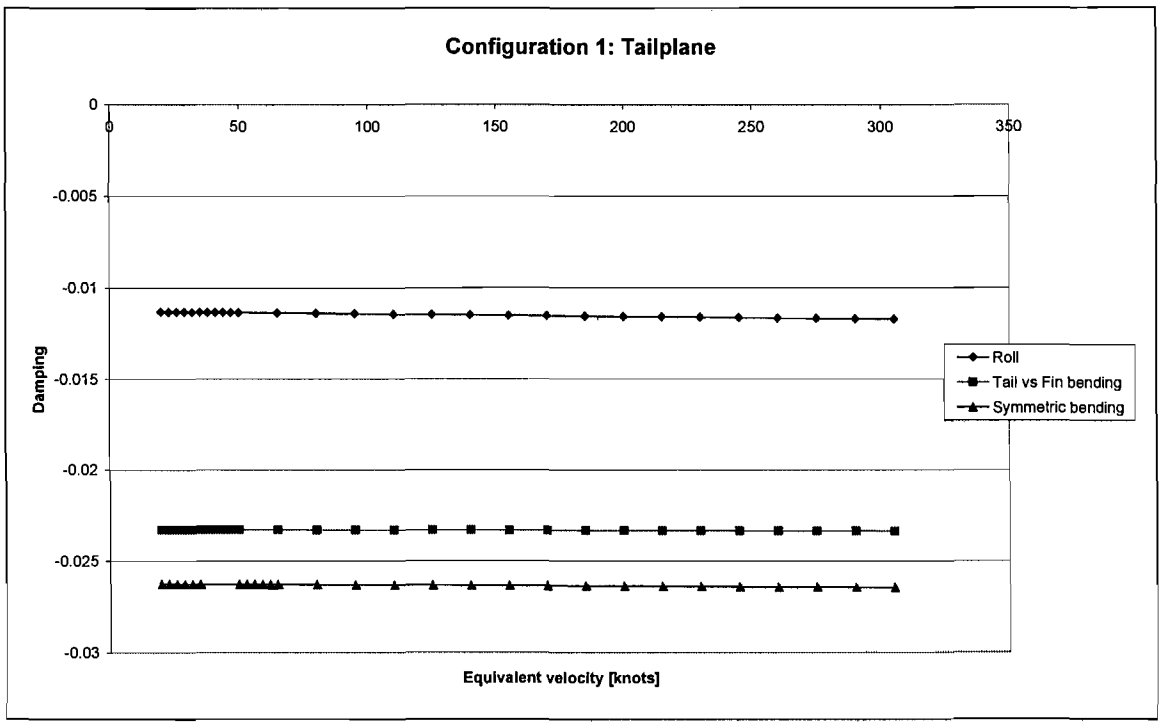
Configuration 1: Tailplane
0
0
50
100
150
200
250
300
350
-0.005
-0.01
-0.015
-0.02
-0.025
-0.03
Damping
Roll
Tail vs Fin bending
Symmetric bending
Equivalent velocity [knots]

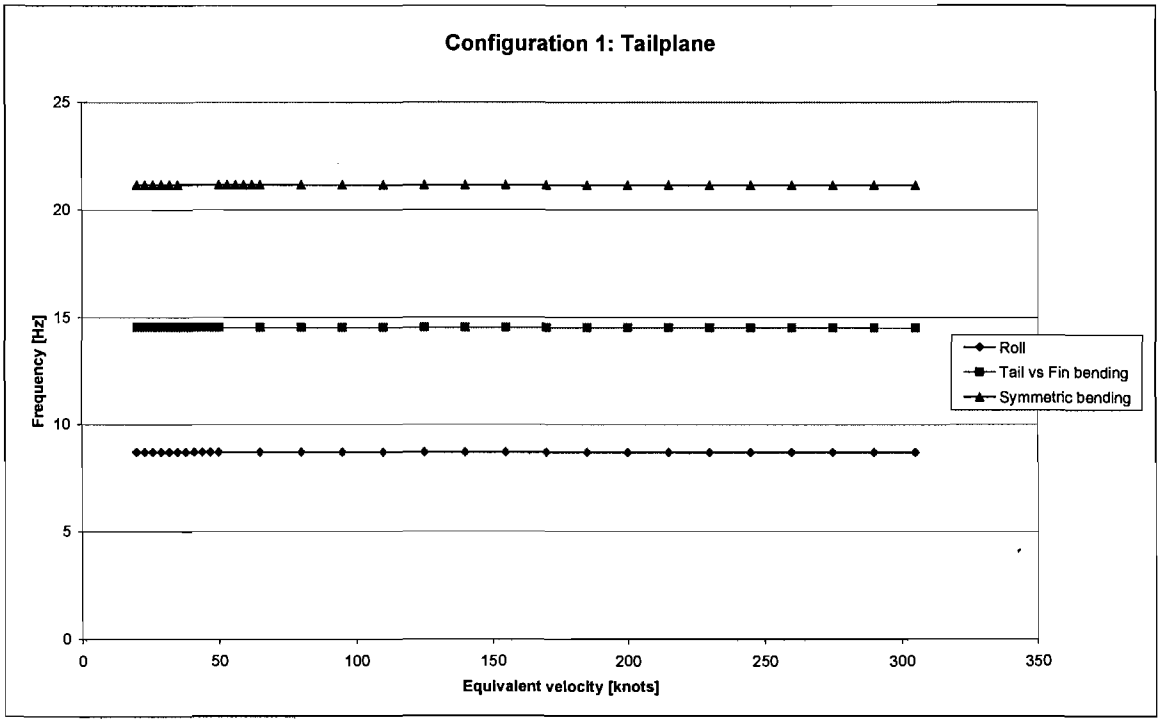
Configuration 1: Tailplane
25
20
15
10
5
0
Frequency [Hz]
0
50
100
150
200
250
300
350
Roll
Tail vs Fin bending
Symmetric bending
Equivalent velocity [knots]

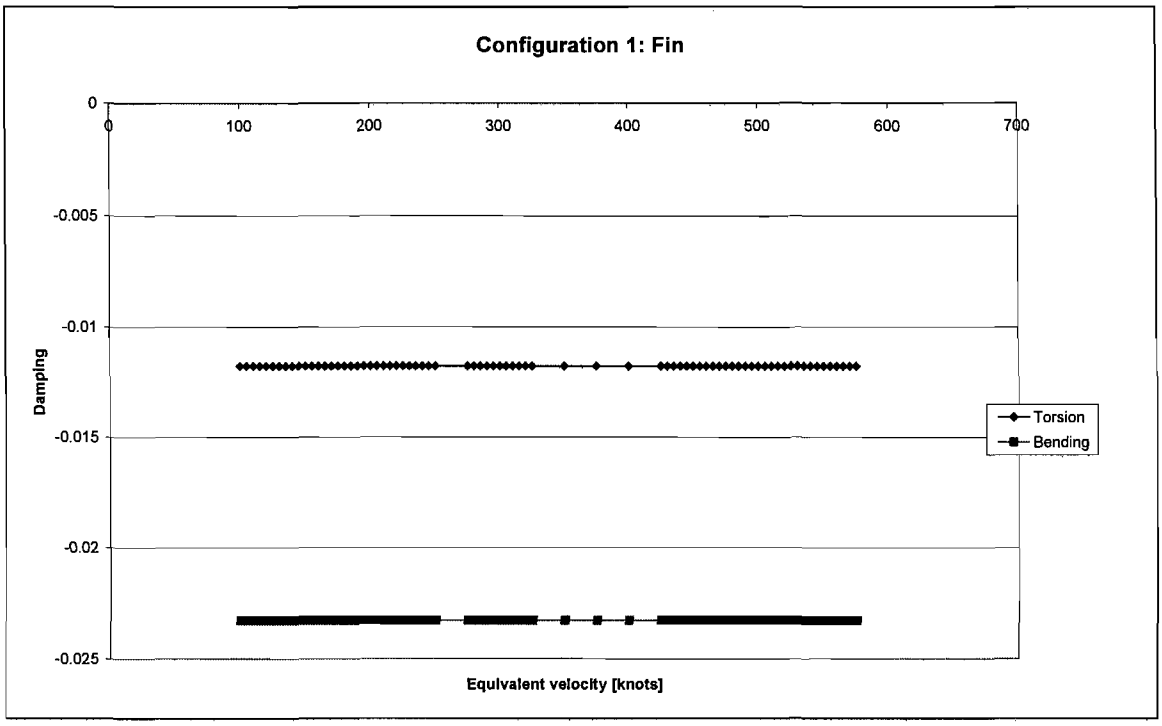
Configuration 1: Fin
0
-0.005
-0.01
-0.015
-0.02
-0.025
Damping
0
100
200
300
400
500
600
700
Equivalent velocity [knots]
Torsion
Bending

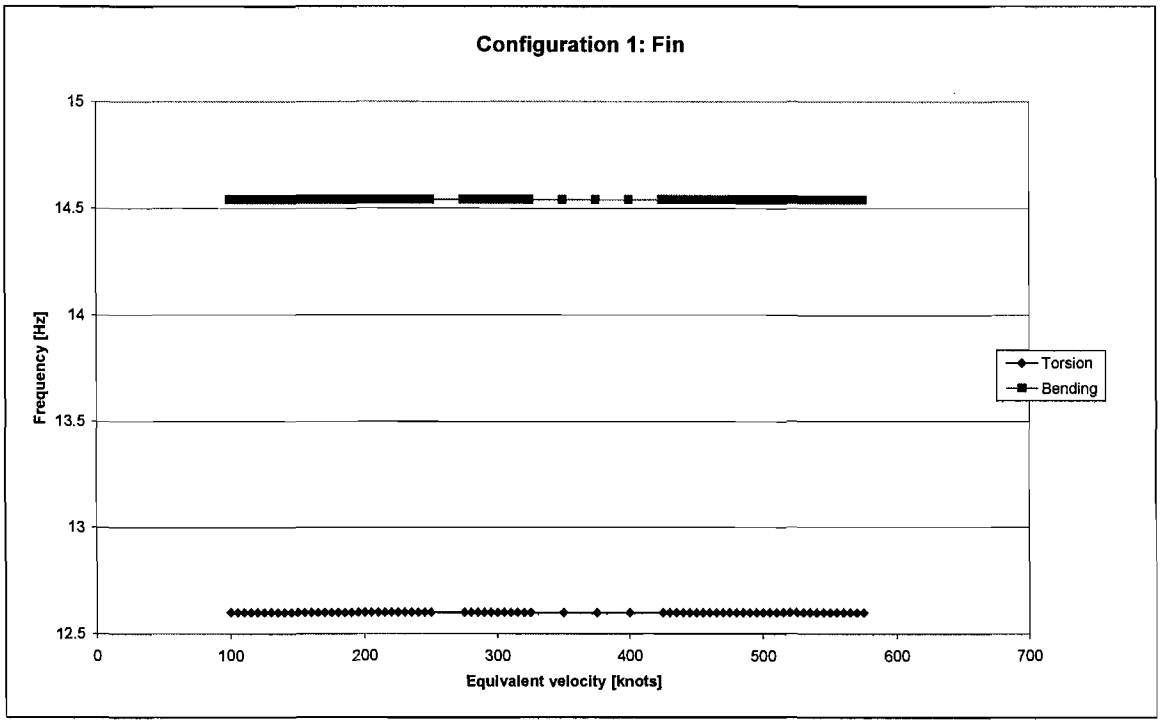
Configuration 1: Fin
15
14.5
14
13.5
13
12.5
Frequency [Hz]
0
100
200
300
400
500
600
700
Equivalent velocity [knots]
Torsion
Bending

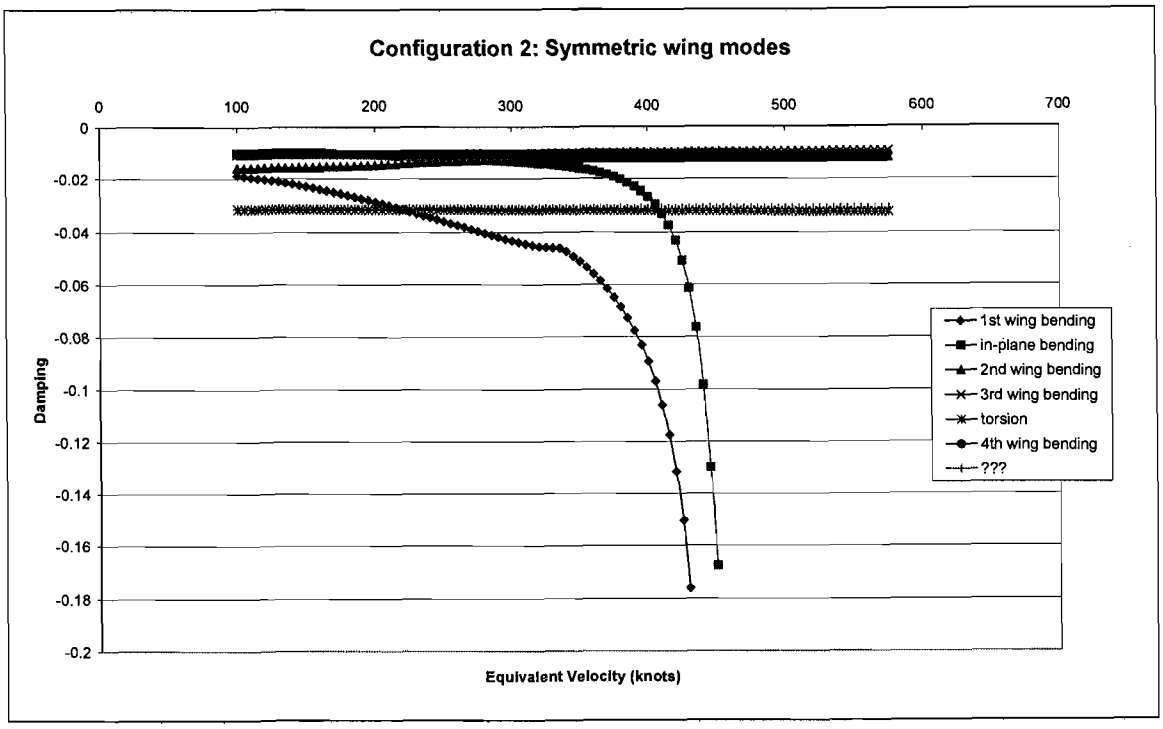
Configuration 2: Symmetric wing modes
0
100
200
300
400
500
600
700
0
-0.02
-0.04
-0.06
-0.08
-0.1
-0.12
-0.14
-0.16
-0.18
-0.2
Damping
Equivalent Velocity (knots)
1st wing bending
in-plane bending
2nd wing bending
3rd wing bending
torsion
4th wing bending
???

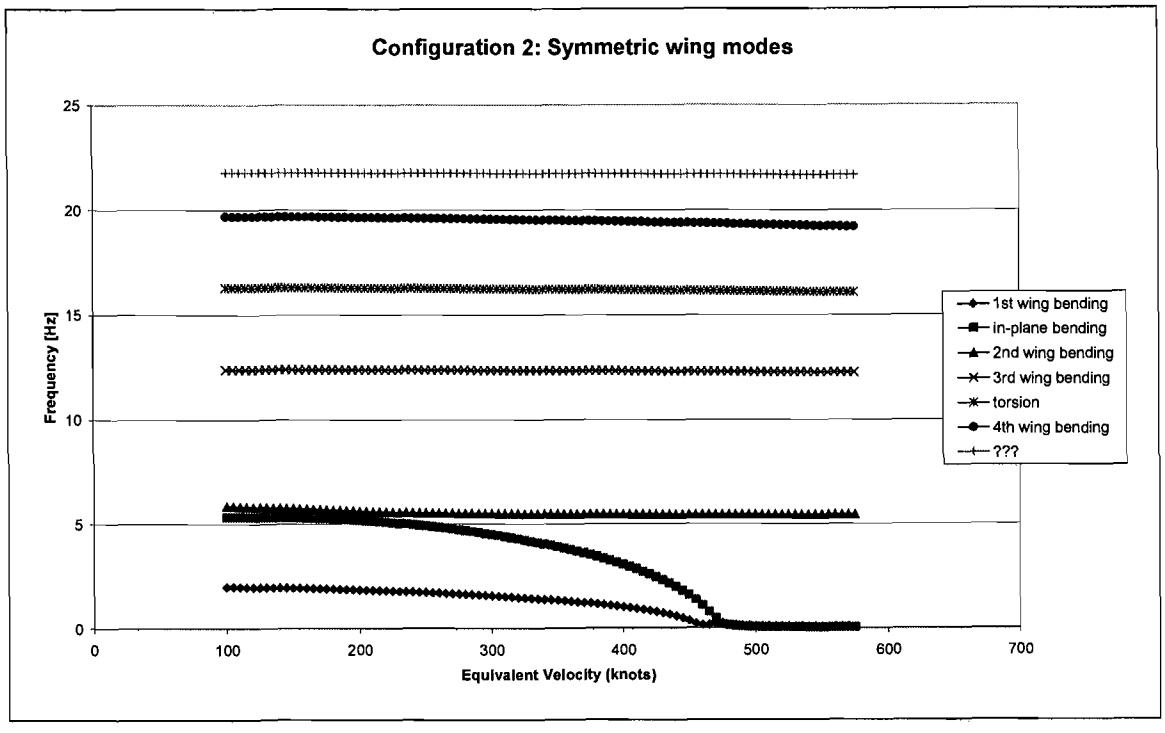
Configuration 2: Symmetric wing modes
25
20
15
10
5
0
Frequency [Hz]
0
100
200
300
400
500
600
700
Equivalent Velocity (knots)
1st wing bending
in-plane bending
2nd wing bending
3rd wing bending
torsion
4th wing bending
???

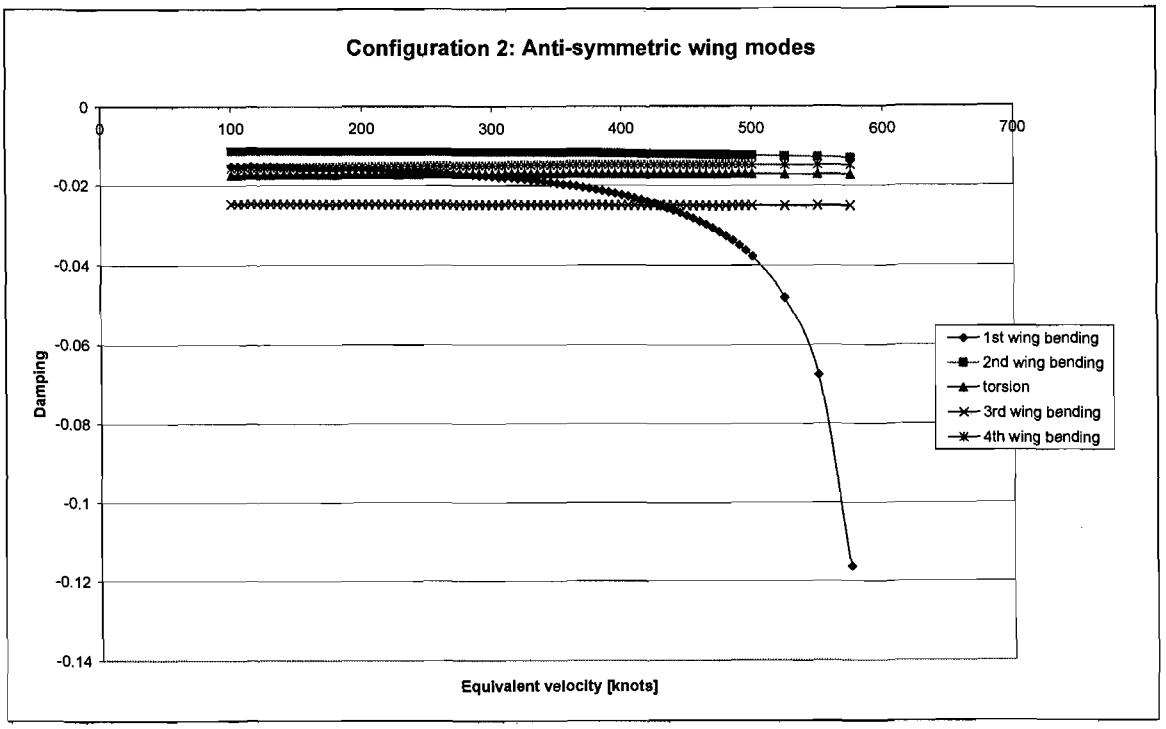
Configuration 2: Anti-symmetric wing modes
0
-0.02
-0.04
-0.06
-0.08
-0.1
-0.12
-0.14
Damping
0
100
200
300
400
500
600
700
Equivalent velocity [knots]
1st wing bending
2nd wing bending
torsion
3rd wing bending
4th wing bending

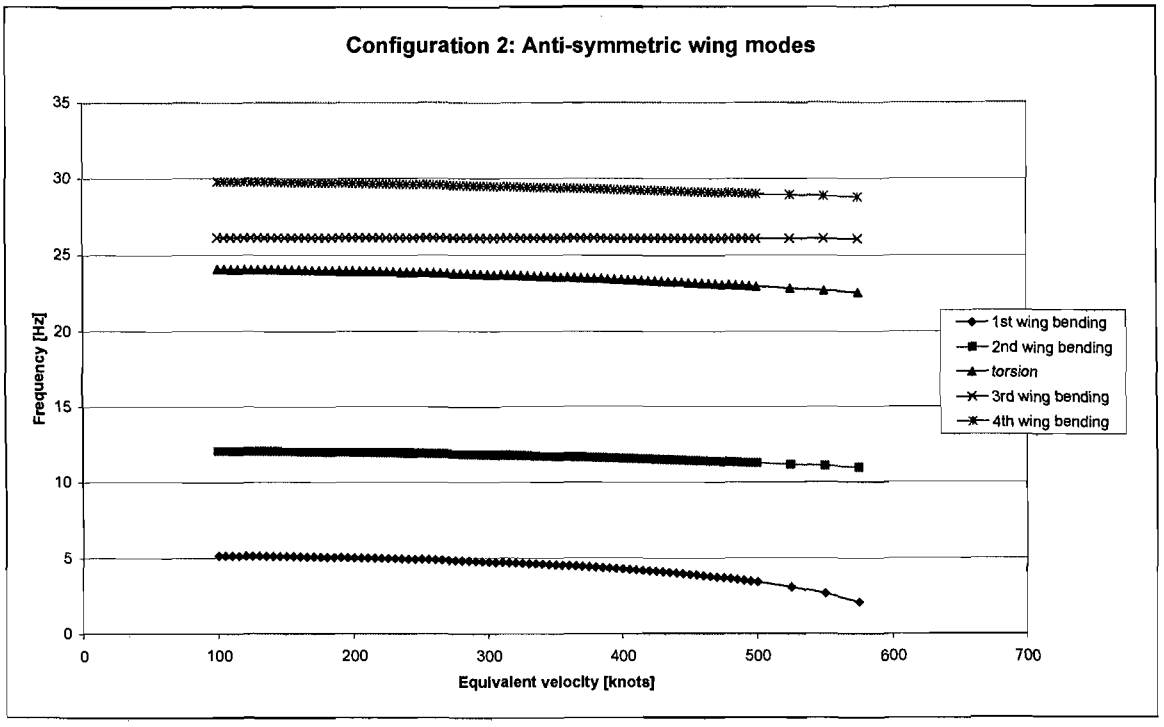
Configuration 2: Anti-symmetric wing modes
35
30
25
20
15
10
5
0
Frequency [Hz]
0
100
200
300
400
500
600
700
Equivalent velocity [knots]
1st wing bending
2nd wing bending
torsion
3rd wing bending
4th wing bending

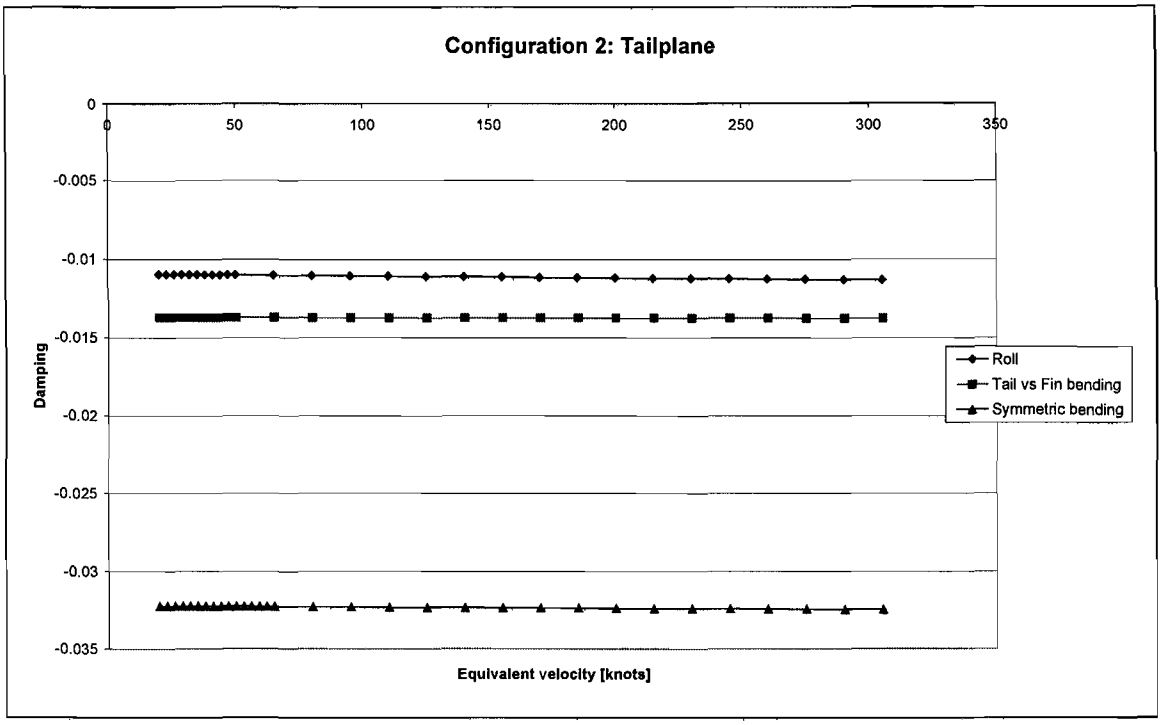
Configuration 2: Tailplane
0
-0.005
-0.01
-0.015
-0.02
-0.025
-0.03
-0.035
Damping
0
50
100
150
200
250
300
350
Equivalent velocity [knots]
Roll
Tail vs Fin bending
Symmetric bending

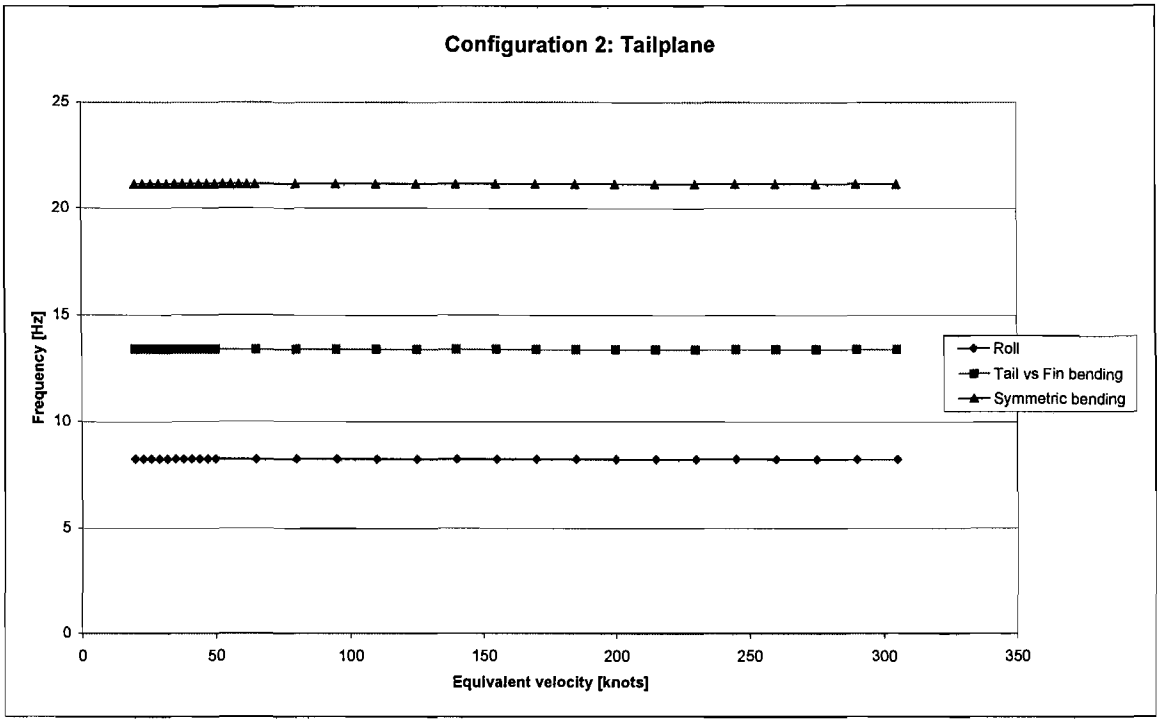
Configuration 2: Tailplane
25
20
15
10
5
0
Frequency [Hz]
0
50
100
150
200
250
300
350
Equivalent velocity [knots]
Roll
Tail vs Fin bending
Symmetric bending

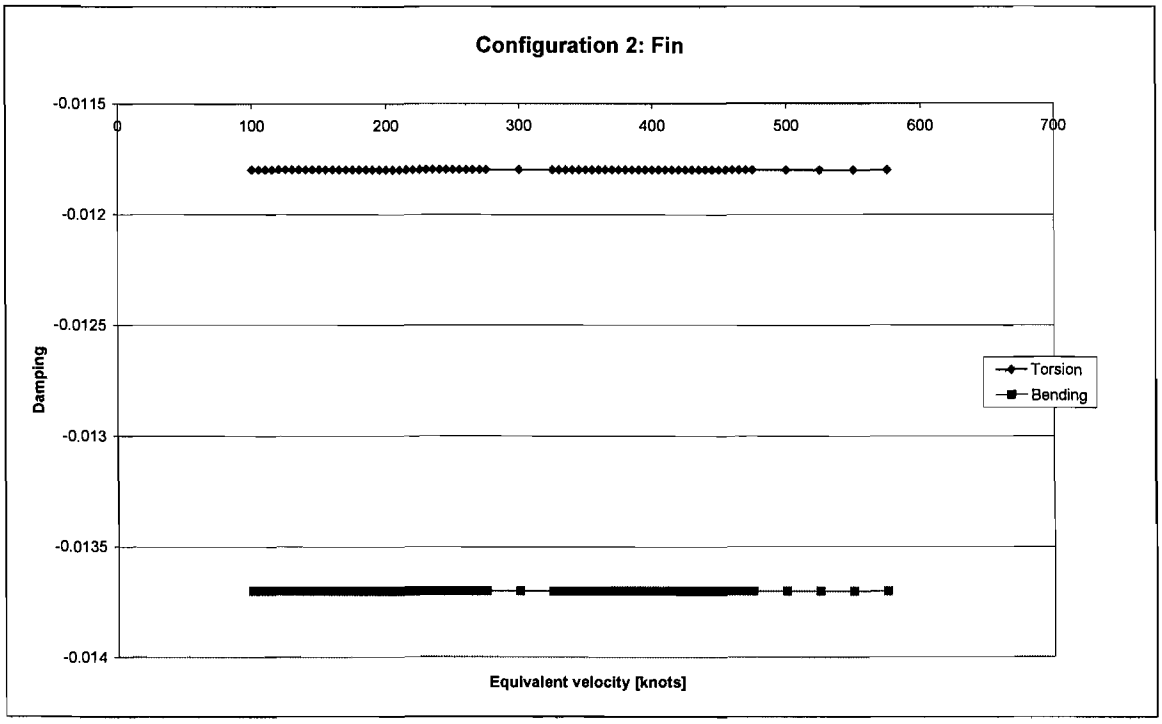
Configuration 2: Fin
-0.0115
-0.012
-0.0125
-0.013
-0.0135
-0.014
Damping
0
100
200
300
400
500
600
700
Torsion
Bending
Equivalent velocity [knots]

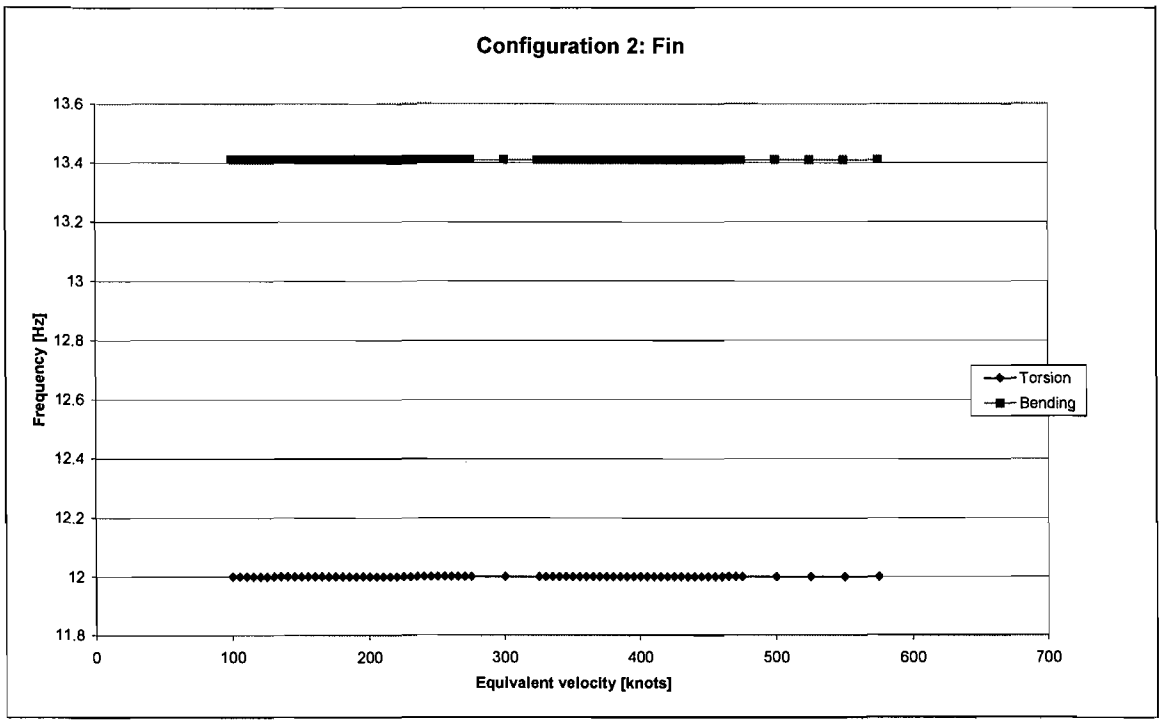
Configuration 2: Fin
13.6
13.4
13.2
13
12.8
12.6
12.4
12.2
12
11.8
Frequency [Hz]
0
100
200
300
400
500
600
700
Torsion
Bending
Equivalent velocity [knots]

# 7 BIBLIOGRAPHY

BRENNER, M.J., LIND, R.C., VORACEK, D.F. 1997. Overview of recent flight flutter testing research at NASA Dryden. *NASA Technical Memorandum 4792*, 1-27, April.

CARSON III, J.M., ALVAREZ, E., DANIELS, A.T. 1997. Ground vibration test of a Star-Lite aircraft. Austin : University of Texas at Austin (Final Report) 100p.

Certification Specifications. 2003. CS-22 for sailplanes and powered sailplanes. European Aviation Safety Agency. Germany.

DE BRUYN, J.A. 2004. A preliminary theoretical flutter analysis of the JS1 glider. Potchefstroom : NWU (Thesis – M.Eng) 71 p.

DOWELL, E.H., CRAWLEY, E.F., CURTISS, Jr. H.C., PETERS, D.A., SCANLAN, R.H. & SISTO, F. 1995. A modern course in aeroelasticity. Dordrecht : Kluwer Academic Publishers. 699 p.

DUNCAN, W.J. 1945. The fundamentals of flutter. Aircraft Engineering, 17: 16-20, Jan., 32-38, Feb.

FUNG, F.C. 1969 [1993]. An introduction to the theory of aeroelasticity. New York : Dover Publications, Inc. 498 p.

HEWLETT PACKARD. 1997. The fundamentals of modal testing. Application Note 243-3, 1992.

HODGES, D.H. & PIERCE, G.A. 2002. Introduction to structural dynamics and aeroelasticity. Cambridge : Cambridge University Press. 167 p.

HOLLMANN, M. 1997. Modern aerodynamic flutter analysis. 2nd ed. Monterey, California : Aircraft Designs, Inc. 168 p.

JAMES, M.L., SMITH, G.M., WOLFORD, J.C., & WHALEY, P.W. 1989. Vibration of mechanical and structural systems: With microcomputer applications. New York : Harper & Row Publishers. 652 p.

KEHOE, M.W. 1995. A historical overview of flutter flight testing. *NASA Technical Memorandum 4720*, 1-7, Oct.

LIND, R.C. 2002. Flight test evaluation of flutter prediction methods. Journal of aircraft, 40(5):964-970, Oct.

RAO, S.S. 2004. Mechanical vibration. New Jersey : Pearson Prentice Hall. 1078 p.

RICHARDSON, M.H. & SCHWARZ, B.J. 1999. Experimental modal analysis. CSI Reliability Week, Orlando, FL. Oct. 1999. 12 p.

SHOKRIEH, M.M. & BEHROOZ, F.T. 2001. Wing instability of a full composite aircraft. *Composite Structures*. 54:335-340.

TEWARI, A. 1999. Flutter: The flying Nemesis. [Web:] http://www.iitk.ac.in/infocell/Archive/dirjan1/flutter.html [11 June 2007]

Van Zyl, L.H. (LvZyl@csir.co.za) 2007. Glider support system. [E-mail to:] Rossouw, P.S. (12528625@nwu.ac.za) Feb. 93.

ZIENKIEWICZ, O.C. & TAYLOR, R.L. 2000. The finite element method. 5th edition. Oxford : Butterworth-Heinemann. 689 p.